석사 학위논문
Master's Thesis

파랑-구조 상호작용 문제에서 비정상 주파수 현상 검출

On the Irregular Frequency Phenomenon in Wave-Structure Interaction Problem

김 산 (金 山 Kim, San)
기계항공시스템학부 해양시스템공학전공
School of Mechanical, Aerospace and Systems Engineering,
Division of Ocean Systems Engineering

KAIST

2015

파랑-구조 상호작용 문제에서 비정상 주파수 현상 검출

On the Irregular Frequency Phenomenon in Wave-Structure Interaction Problem

On the Irregular Frequency Phenomenon in Wave-Structure Interaction Problem

Advisor : Professor Lee, Phill-Seung

By

Kim, San
School of Mechanical, Aerospace and Systems Engineering,
Division of Ocean Systems Engineering
KAIST

A thesis submitted to the faculty of KAIST in partial fulfillment of the requirements for the degree of Master of Science and Engineering in the School of Mechanical, Aerospace and Systems Engineering, Division of Ocean Systems Engineering. The study was conducted in accordance with Code of Research Ethics[1]

2014. 12. 16

Approved by

Professor Lee, Phill-Seung

[1] Declaration of Ethical Conduct in Research: I, as a graduate student of KAIST, hereby declare that I have not committed any acts that may damage the credibility of my research. These include, but are not limited to: falsification, thesis written by someone else, distortion of research findings or plagiarism. I affirm that my thesis contains honest conclusions based on my own careful research under the guidance of my thesis advisor.

파랑-구조 상호작용 문제에서 비정상 주파수 현상 검출

김 산

위 논문은 한국과학기술원 석사학위논문으로
학위논문심사위원회에서 심사 통과하였음.

2014 년 12 월 16 일

심사위원장 이 필 승 (인)

심사위원 최 우 영 (인)

심사위원 조 연 우 (인)

MOSE
20133097

김 산. Kim, San. On the Irregular Frequency Phenomenon in Wave-Structure Interaction Problems. 파랑-구조 상호작용 문제에서 비정상 주파수 현상 검출. School of Mechanical Aerospace and Systems Engineering, Division of Ocean Systems Engineering. 2015. 52 p. Advisor Prof. Lee, Phill-Seung.

ABSTRACT

Wave-structure interaction problem is important in ship and offshore engineering. Linear potential theory is used widely for numerical analysis of wave-structure interaction problem. However, in the frequency domain analysis using the linear potential theory, error occurs at certain wave frequencies are called the irregular frequencies. These frequencies do not represent the physical resonance such as sloshing but are due to the uniqueness of solution of boundary integral equation.

We define the irregular frequency and introduce the extended boundary integral equation (EBIE) method that is one of irregular frequency removal (IRR) methods. The EBIE method that guarantees the uniqueness of the boundary integral equation for wave-structure interaction problem is applicable to three-dimensional body of arbitrary shape but it increases computational cost according to the degree of freedom on the wet-surface and interior free-surface. To reduce the increment of computational cost due to the EBIE method, we present the cost reduction procedure for IRR method. This procedure apply the EBIE method selectively by detecting wave frequencies that are affected by the irregular frequencies. The feasibility is shown by applying the cost reduction procedure to examples: barge, circular cylinder, and ship-shaped offshore unit.

Keywords: Wave-structure interaction; Liner potential theory; Boundary integral equation; free-surface Green function; Irregular frequency; Fredholm’s theorem; Extended boundary integral equation method

Table of Contents

List of Tables

List of Figures

Chapter 1. Introduction

1.1 Research Background

Analysis of free-surface wave structure interaction problem such as the rigid body motions of ship and the hydroelastic behavior of floating structure is practically important in offshore engineering for the design of offshore structures and the safe operation. In the linearized frequency domain analysis, the linear potential theory is widely used. Utilizing the Green theorem, the linear potential theory induces the boundary integral equation formulation. It is generally accepted that the boundary integral equation breaks down at specific wave frequencies that are called the irregular frequencies. Roughly speaking, the irregular frequencies are related to the volume of displacement and the shape of floating structure. As the volume of displacement increases, irregular frequencies decrease and come within wave frequency range of interest. Additionally, error of numerical solution due to irregular frequencies is similar to physical resonance peak of sloshing and multibody problem [1], so analysis of ships and floating structures should consider the irregular frequencies for accurate analysis result.

The occurrence of the irregular frequencies in the field of acoustic was first reported by Lamb in 1932 [2]. In the field of waves and structures interaction, John recognized the existence of the irregular frequencies in 1949 [3]. Several methods have been proposed to remove the irregular frequency effect. Broadly speaking, the irregular frequency removal method can be divided into two categories [4]:

- Modification of the integral operator
- Modification of the domain of the integral operator.

Several methods of modification of the integral operator methods have been adapted in wave-structure interaction problem. Ursell [5] added a source at the origin to absorb the energy of the interior eigenmodes. Lee and Sclavounos [6] adapted Modified integral equation method. The additional integral equation is added to the boundary integral equation. The additional equation is the differentiation of the boundary integral equation with respect to the field point. Modification of the domain of the integral operator method also has been adapted into wave-structure interaction problem. The concept of this method is suppressing the interior eigenmodes by placing the lid on the interior freesurface. Each method has its pros and cons in terms of generality, computational cost, and modeling effort. WAMIT, widely using for wave-structure interaction problem, includes the Extended Boundary Integral equation(EBIE) method that is one of modification of the domain of the integral operator methods as an irregular frequency removal(IRR) option.

The EBIE method that increases the computational cost is available for general shape ships and floating structures. However, because it is difficult to distinguish the existence of irregular frequencies in the frequency range of interest, the IRR method which increases the computational cost should be adapted to every analysis. Therefore, the total computational cost increases by adapting the IRR method.

1.2 Research Object and Contents

The objective of this research is to present the numerical analysis procedure that adapt the EBIE method selectively to reduce the computational cost.

In the following chapter, we identify the boundary integral equation for rigid body and a direct-coupled equation for flexible floating body and transform into a discrete linear system in chapter 2. In chapter 3, we define the irregular frequencies and find the irregular frequency of barge and circular cylinder analytically. The cost reduction procedure for the IRR method in case of single body problem that does not include sloshing phenomenon is presented in chapter 4. Finally, we evaluate hydrodynamic coefficients of barge, circular cylinder, and ship-shaped offshore unit to show the feasibility of the cost reduction procedure for the IRR method. The numerical solutions in chapter 5 are obtained using source code developed by CMSS laboratory in KAIST, a three dimensional hydroelastic analysis code using a direct-coupling method of waves and floating structures [7, 8]. Chapter 6 draws the conclusions.

Chapter 2. Mathematical Formulation and Numerical Method

This chapter describes the assumptions and governing equations. First, we present the boundary value problem, and then we derive the boundary integral equation that has the irregular frequencies. Second, we briefly review the direct-coupled equations for hydroelastic analysis and the discrete version of the direct-coupled equations.

2.1 Overall Description and Assumptions

We consider a three-dimensional floating structure which interacts with plane progressive wave as shown in Figure 2.1. Cartesian coordinate system of which origin is located on the free-surface is used. The water depth is h. The wave incident angle θ is an angle between two lines: positive x_1 direction line and incident wave direction line. We adopt a harmonic time dependence and assume that the motion of floating structures and the amplitude of wave are small compared to the characteristic length of floating structures and wave length respectively. Assuming newtonian isotropic, incompressible, inviscid and irrotational fluid, we use the linear potential flow to describe free-surface waves.

2.2 Modeling of the Fluid

We confine our discussion to a three-dimensional floating structure, which interacts with small amplitude wave, so we use the linear potential flow for mathematical model of incident wave. We simplified the fluid domain for the linear potential flow formulation from the problem description of Figure 2.2. Boundaries, which surround the fluid domain, consist of four surfaces: the wet-surface (S_B), the infinite boundary (S_∞) , the bottom boundary (S_G), and the free-surface (S_F).

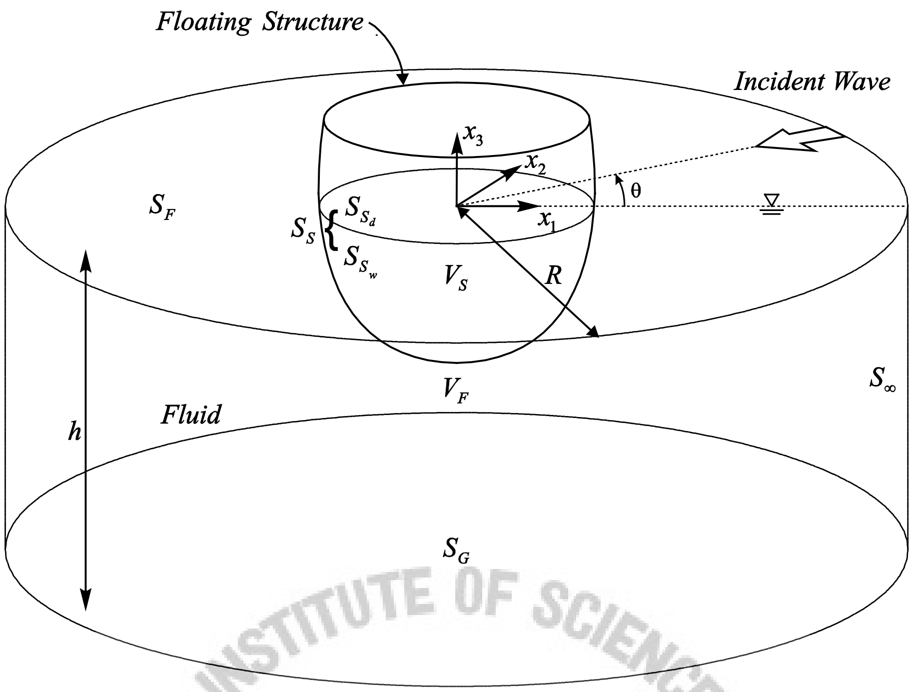

Figure 2.1. Problem description for free-surface wave structure interaction.

In general, the radiation and diffraction potentials are dealt with separately when the motions of rigid floating structures are analyzed. By integrating the radiation potential, we can get an added mass and a wave damping coefficients for the equation of rigid body motion. A wave exciting force can be obtained through integration of the diffraction potential. Meanwhile, the total potential, which is sum of the radiation and diffraction potentials, is used for the analysis of a hydroelastic behavior of floating structure in the direct-coupled equation [7]. In this thesis, discussion would continue based on the direct-coupled formulation, so the total potential would be dealt with in the next section.

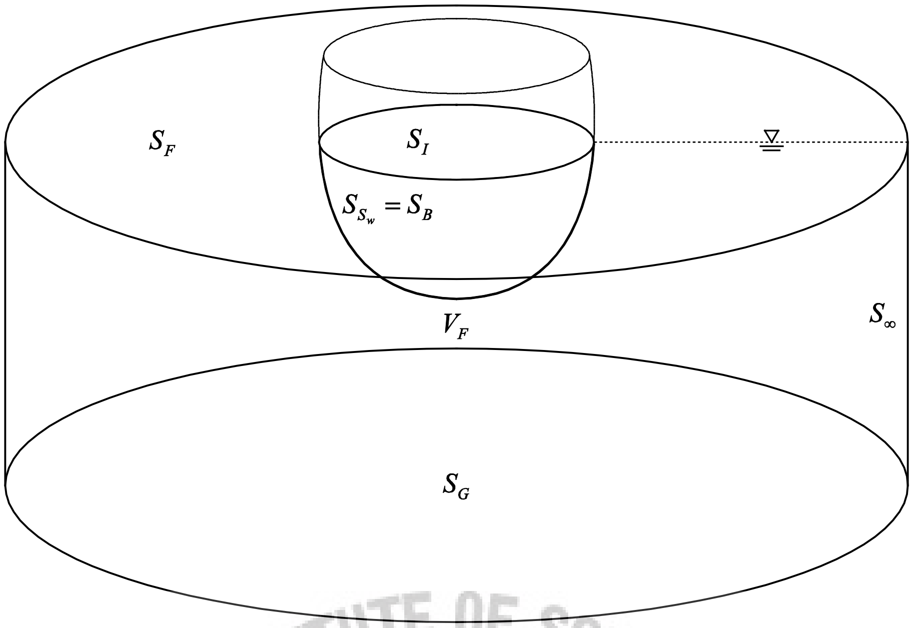

Figure 2.2. Fluid domain of wave-floating structure interaction problem.

2.2.1 Boundary Value Problem (Exterior Neumann Problem)

We assumed a harmonic time dependence, so we define the velocity potential as ${}^{\tau}\phi = \mathrm{Re}\left\lfloor \phi e^{j\omega t} \right\rfloor$ with the time factor $e^{j\omega t}$ in the fluid domain as shown in Figure 2.2. ω is the frequency of free-surface wave and j is $\sqrt{-1}$. With the continuity equation and the assumption ideal flow and time dependence, we starts with the velocity potential which satisfies the Laplace's equation:

$$\nabla^2 \phi. \tag{2.1}$$

The velocity potential satisfies the linearized free-surface boundary condition:

$$\frac{\partial \phi}{\partial x_3} = \frac{\omega^2}{g}\phi, \qquad \text{for } x_3 = 0 \text{ on } S_F \tag{2.2}$$

the bottom boundary condition:

$$\frac{\partial \phi}{\partial x_3} = 0, \qquad \text{on } S_G \ (x_3 = -h) \tag{2.3}$$

the radiation condition:

$$\sqrt{R}\left(\frac{\partial}{\partial R} + jk\right)(\phi - \phi_I = 0), \qquad \text{on } S_\infty \quad (R \to \infty) \tag{2.4}$$

the body boundary condition:

$$\frac{\partial \phi}{\partial n} = j\omega u_i n_i, \qquad \text{on } S_B \qquad (2.5)$$

where $\mathbf{u}$ is the displacement of the floating structure, $\mathbf{n}$ is the unit normal vector on S_B, $(\phi - \phi_I)$ is the sum of radiation and scattering potential, and k is the wave number. From now on, we refer this boundary value problem as the exterior Neumann problem because of its domain and boundary condition on S_B.

The incident wave potential ϕ_I is defined by

$$\phi_I = j\frac{ga}{\omega} e^{kx_3} e^{jk(x_1 \cos\theta + x_2 \sin\theta)} \qquad (2.6)$$

for the infinite depth where a is an amplitude of the incident wave [9].

The above boundary value problem could be solve by using the boundary integral equation method. To derive the boundary integral equation, we use the free-surface Green function. The free-surface Green function is the potential at the field point $\mathbf{x}$ due to a source at the source point ξ. It pulsates with the angular frequency ω, and satisfies the Laplace's equation:

$$\nabla^2 G(\mathbf{x} - \xi) = -4\pi\delta(\mathbf{x} - \xi) \qquad \text{for } -h \le x_3 \le 0 \qquad (2.7)$$

where $G(\mathbf{x};\xi)$ is defined as ${}^{\tau}G(\mathbf{x};\xi,\omega) = \mathrm{Re}\left[G(\mathbf{x};\xi)e^{j\omega t}\right]$ and δ is the Dirac's delta function.

It also satisfies the linearized free-surface boundary condition:

$$\frac{\partial G}{\partial x_3} = \frac{\omega^2}{g} G, \qquad \text{for } x_3 = 0 \text{ and } x_i \ne \xi_i \qquad (2.8)$$

the bottom boundary condition:

$$\frac{\partial G}{\partial x_3} = 0, \qquad \text{for } x_3 = -h \text{ and } x_i \ne \xi_i \qquad (2.9)$$

the radiation condition:

$$\sqrt{r}\left(\frac{\partial}{\partial r} + jk\right) G = 0, \qquad \text{on } S_\infty \quad (r \to \infty) \qquad (2.10)$$

where $r = \sqrt{(x_1 - \xi_1)^2 + (x_2 - \xi_2)^2}$.

Derivation procedure of the free-surface Green's function in finite and infinite depth is well explained by Wehausen and Laitone [10]. In case of infinite depth, the free-surface Green function is

$$G(\mathbf{x};\boldsymbol{\xi}) = \frac{1}{\sqrt{R^2 + (x_3 - \xi_3)^2}} + P.V.\int_0^\infty \left[\frac{z + (\omega^2/g)}{z - (\omega^2/g)} e^{-z|x_3+\xi_3|} J_0(zR) \right] dz$$

$$- 2\pi \frac{\omega^2}{g} e^{-(\omega^2/g)|x_3+\xi_3|} J_0\left(\left(\frac{\omega^2}{g} \right) R \right) j, \tag{2.11}$$

where $P.V.$ means the Cauchy principal value, and J_0 is Bessel functions of the first kind of order 0. In case of finite depth, the free-surface Green function is

$$G(\mathbf{x};\boldsymbol{\xi}) = \frac{1}{\sqrt{R^2 + (x_3 - \xi_3)^2}} + \frac{1}{\sqrt{R^2 + (2h + x_3 + \xi_3)^2}}$$

$$+ 2P.V.\int_0^\infty \left[\frac{\{z + (\omega^2/g)\} \cosh z(x_3 + h) \cosh z(\xi_3 + h)}{z \sinh zh - (\omega^2/g) \cosh zh} e^{-zh} J_0(zR) \right] dz$$

$$+ 2\pi \frac{\left(\frac{\omega^2}{g} \right)^2 - k_0^{\,2}}{k_0^{\,2} h - \left(\frac{\omega^2}{g} \right)^2 h + \left(\frac{\omega^2}{g} \right)} \cosh k_0 (x_3 + h) \cosh k_0 (\xi_3 + h) J_0(k_o R) j \tag{2.12}$$

where k_0 means the positive real root of the dispersion relation equation, $\omega^2 = gk \tanh(kh)$.

2.2.2 Boundary Integral Equation

To derive the boundary integral equation to solve the above boundary value problem, we starts with the Green's theorem. If two arbitrary potential ϕ_1 and ϕ_2 satisfy the Laplace's equation in the domain of fluid, the following equation:

$$\int_{S_C} \left[\phi_1 \frac{\partial \phi_2}{\partial n} - \phi_2 \frac{\partial \phi_1}{\partial n} \right] dS = 0, \tag{2.13}$$

where $\mathbf{n}$ is normal to S_C from the fluid domain, can be derived easily. S_C should be a smooth and closed surface surrounding the fluid domain. When one of the two potential does not satisfy the Laplace's equation in the fluid domain, some technique that modify the fluid domain and use the singularity property can be applied [11]. The result equations are following:

$$\int_{S_C} \left[\phi(\boldsymbol{\xi}) \frac{\partial G(\mathbf{x};\boldsymbol{\xi})}{\partial n(\boldsymbol{\xi})} - G(\mathbf{x};\boldsymbol{\xi}) \frac{\partial \phi(\boldsymbol{\xi})}{\partial n(\boldsymbol{\xi})} \right] dS(\boldsymbol{\xi}) = \begin{cases} 0 & \text{for } \mathbf{x} \text{ outside } S_C \\ -2\pi\phi(\mathbf{x}) & \text{for } \mathbf{x} \text{ on } S_C \\ -4\pi\phi(\mathbf{x}) & \text{for } \mathbf{x} \text{ inside } S_C \end{cases} \tag{2.14}$$

When the field point $\mathbf{x}$ is on S_C or inside S_C, this point is excluded by small surface, S_ε surrounding the point. The integration over this small surface appears in the right hand side of equation (2.14).

Let's apply Equation (2.14) for fluid domain V_F surrounded by surfaces: S_B, S_F, S_G, and S_∞ as shown in Figure 2.3, and then we obtain

$$2\pi\phi(\mathbf{x})+\int_{S_B+S_F+S_G+S_\infty}\left[\phi(\xi)\frac{\partial G(\mathbf{x};\xi)}{\partial n(\xi)}-G(\mathbf{x};\xi)\frac{\partial \phi(\xi)}{\partial n(\xi)}\right]dS(\xi)=0 \qquad \text{for } \mathbf{x} \text{ on } S_B \tag{2.15}$$

Because G has the same boundary condition on S_F and S_G with ϕ, and on S_∞ with $(\phi-\phi_I)$, so we get

$$\begin{aligned}-2\pi\phi(\mathbf{x})=&\int_{S_B}\left[\phi(\xi)\frac{\partial G(\mathbf{x};\xi)}{\partial n(\xi)}-G(\mathbf{x};\xi)\frac{\partial \phi(\xi)}{\partial n(\xi)}\right]dS(\xi)\\&+\int_{S_\infty}\left[\phi_I(\xi)\frac{\partial G(\mathbf{x};\xi)}{\partial n(\xi)}-G(\mathbf{x};\xi)\frac{\partial \phi_I(\xi)}{\partial n(\xi)}\right]dS(\xi)\end{aligned} \qquad \text{for } \mathbf{x} \text{ on } S_B \tag{2.16}$$

Next, consider the fluid domain V surrounded by surfaces: S_F, S_I, S_G and S_∞ as shown in Figure 2.4, and then we obtain

$$4\pi\phi_I(\mathbf{x})+\int_{S_F+S_I+S_G+S_\infty}\left[\phi_I(\xi)\frac{\partial G(\mathbf{x};\xi)}{\partial n(\xi)}-G(\mathbf{x};\xi)\frac{\partial \phi_I(\xi)}{\partial n(\xi)}\right]dS(\xi)=0 \qquad \text{for } \mathbf{x} \text{ on } S_B \tag{2.17}$$

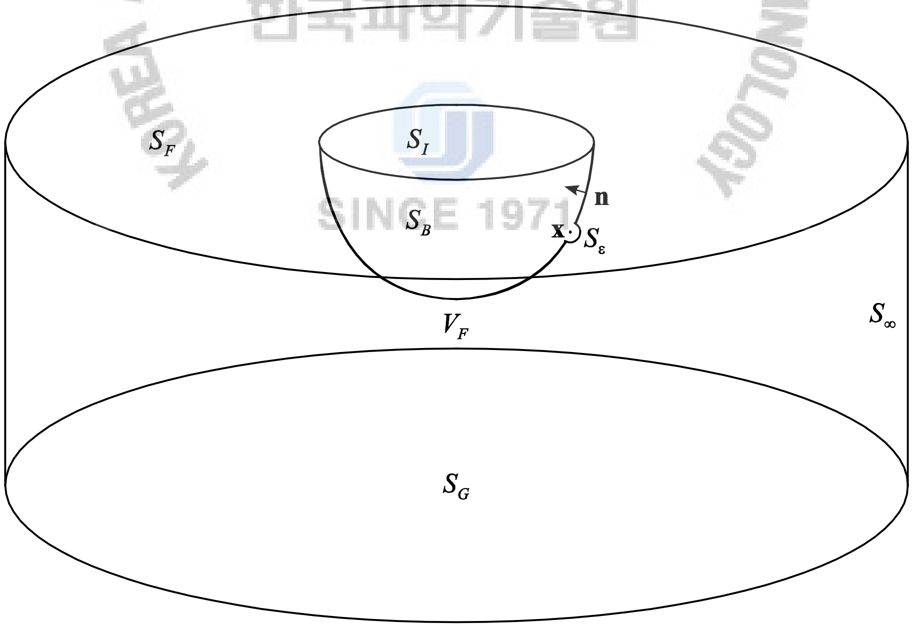

Figure 2.3. Fluid domain V_F when $\mathbf{x}$ is on S_B.

Integration over S_F and S_I disappear due to the linearized free-surface and bottom boundary conditions of

ϕ_I and G, so we have

$$-4\pi\phi_I(\mathbf{x}) = \int_{S_\infty}\left[\phi_I(\xi)\frac{\partial G(\mathbf{x};\xi)}{\partial n(\xi)} - G(\mathbf{x};\xi)\frac{\partial \phi_I(\xi)}{\partial n(\xi)}\right]dS(\xi). \qquad \text{for } \mathbf{x} \text{ on } S_B \qquad (2.18)$$

Finally, by adding Equations (2.16) and (2.18) we obtain following equation:

$$-2\pi\phi(\mathbf{x}) + 4\pi\phi_I(\mathbf{x}) = \int_{S_B}\left[\phi(\xi)\frac{\partial G(\mathbf{x};\xi)}{\partial n(\xi)} - G(\mathbf{x};\xi)\frac{\partial \phi(\xi)}{\partial n(\xi)}\right]dS(\xi) \qquad \text{for } \mathbf{x} \text{ on } S_B \qquad (2.19)$$

and variational equation:

$$\begin{aligned} -\int_{S_B} 2\pi\phi(\mathbf{x})\bar{\phi}(\mathbf{x})dS(\mathbf{x}) + \int_{S_B} 4\pi\phi_I(\mathbf{x})\bar{\phi}(\mathbf{x})dS(\mathbf{x}) = \\ \int_{S_B}\int_{S_B}\left[\phi(\xi)\frac{\partial G(\mathbf{x};\xi)}{\partial n(\xi)} - G(\mathbf{x};\xi)\frac{\partial \phi(\xi)}{\partial n(\xi)}\right]dS(\xi)\bar{\phi}(\mathbf{x})dS(\mathbf{x}) \end{aligned} \qquad (2.20)$$

where $\bar{\phi}$ is the virtual velocity potential.

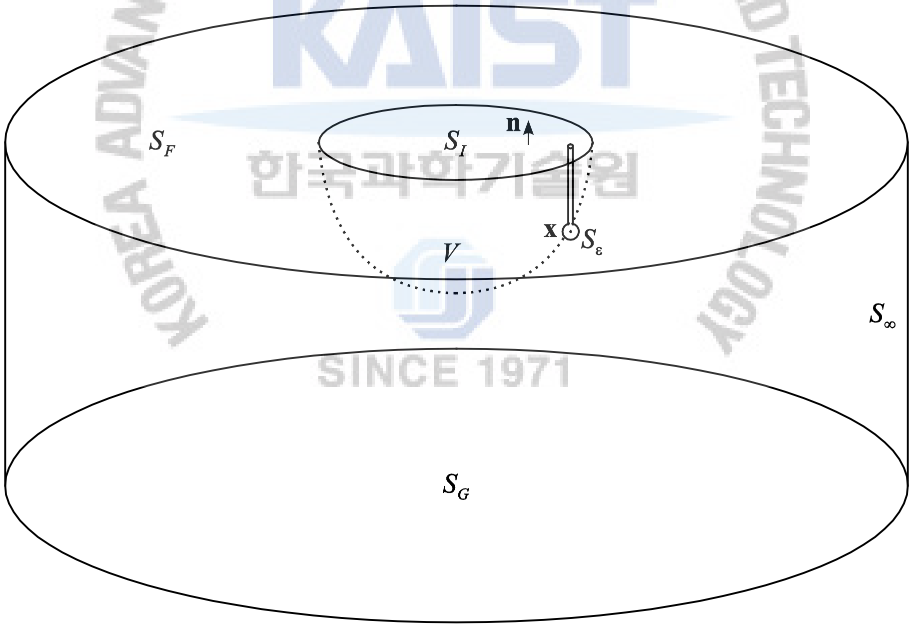

Figure 2.4. Fluid domain V when $\mathbf{x}$ is on S_B.

2.3 Discrete Linear System of Equations

Equation (2.20) representing the boundary value problem of the wave structure interaction cannot be solve alone, because it possess the variable not only the total potential but also the displacement of the structure on the wet surface. To solve the equation, the structure equation that has the same variables should be considered simultaneously, and two equations consist the direct coupled equations. Additionally, for arbitrary shape floating structure the direct coupled equation cannot be solve analytically. Therefore, we use the numerical method. With the finite element discretization and boundary element discretization[7, 12], we can derive the discrete linear system of equation:

$$\begin{bmatrix} -\omega^2\mathbf{S}_M + \mathbf{S}_K + \mathbf{S}_{KN} - \mathbf{S}_{HD} - \mathbf{S}_{HN} & -j\omega\mathbf{S}_D \\ j\omega\mathbf{F}_G & 2\pi\mathbf{F}_M - \mathbf{F}_{Gn} \end{bmatrix} \begin{bmatrix} \hat{\mathbf{u}} \\ \hat{\boldsymbol{\varphi}} \end{bmatrix} = \begin{bmatrix} 0 \\ 4\pi\mathbf{R}_I \end{bmatrix} \tag{2.22}$$

where

$$2\pi\int_{S_B}\phi(\mathbf{x})\bar{\phi}(\mathbf{x})dS(\mathbf{x}) = \hat{\bar{\boldsymbol{\varphi}}}^{\mathrm{T}}[2\pi\mathbf{F}_M]\hat{\boldsymbol{\varphi}}, \tag{2.23a}$$

$$\int_{S_B}\int_{S_B}\left[\phi(\xi)\frac{\partial G(\mathbf{x};\xi)}{\partial n(\xi)}\right]dS(\xi)\bar{\phi}(\mathbf{x})dS(\mathbf{x}) = \hat{\bar{\boldsymbol{\varphi}}}^{\mathrm{T}}[\mathbf{F}_{Gn}]\hat{\boldsymbol{\varphi}}, \tag{2.23b}$$

$$j\omega\int_{S_B}\int_{S_B}[G(\mathbf{x};\xi)u_i(\xi)n_i(\xi)]dS(\xi)\bar{\phi}(\mathbf{x})dS(\mathbf{x}) = \hat{\bar{\boldsymbol{\varphi}}}^{\mathrm{T}}[j\omega\mathbf{F}_G]\hat{\boldsymbol{\varphi}}, \tag{2.23c}$$

$$\int_{S_B}4\pi\phi_I(\mathbf{x})\bar{\phi}(\mathbf{x})dS(\mathbf{x}) = \hat{\bar{\boldsymbol{\varphi}}}^{\mathrm{T}}[4\pi\mathbf{R}_I], \tag{2.23d}$$

for a flexible floating body analysis, and we obtain the fluid part equation:

$$(2\pi\mathbf{F}_M - \mathbf{F}_{Gn})\hat{\boldsymbol{\varphi}} = 4\pi\mathbf{R}_I - j\omega\mathbf{F}_G\hat{\mathbf{u}}. \tag{2.24}$$

In the aforementioned expressions, $\hat{\boldsymbol{\varphi}}$ and $\hat{\mathbf{u}}$ are the nodal velocity potential and displacement vectors, respectively. Equation (2.24) is the discrete linear system of equation corresponds to Equation (2.20) and will be used in the next section to discuss the irregular frequency.

To obtain the discrete linear system of equation for a rigid body motion analysis, we can express the displacement field of rigid body motions by the six degrees of freedom: surge, sway, heave, roll, pitch, and yaw as

$$\begin{aligned} u_i^{R1} &= q_1^R\delta_{1i}, u_i^{R2} = q_2^R\delta_{2i}, u_i^{R3} = q_3^R\delta_{3i} \\ u_i^{R4} &= q_4^R\varepsilon_{ijk}\delta_{1j}x_k, \\ u_i^{R5} &= q_5^R\varepsilon_{ijk}\delta_{2j}x_k, \\ u_i^{R6} &= q_6^R\varepsilon_{ijk}\delta_{3j}x_k. \end{aligned} \tag{2.25}$$

respectively, where ε_{ijk} is the permutation symbol. Then, we can obtain the following discrete linear system of equations:

$$\begin{bmatrix} \mathbf{\Psi}^{RT}\left\{-\omega^2\mathbf{S}_M+\mathbf{S}_K+\mathbf{S}_{KN}-\mathbf{S}_{HD}-\mathbf{S}_{HN}\right\}\mathbf{\Psi}^R & -j\omega\mathbf{\Psi}^{RT}\mathbf{S}_D \\ j\omega\mathbf{F}_G\mathbf{\Psi}^R & 2\pi\mathbf{F}_M-\mathbf{F}_{Gn} \end{bmatrix}\begin{bmatrix}\mathbf{q}\\ \hat{\boldsymbol{\varphi}}\end{bmatrix}=\begin{bmatrix}0\\ 4\pi\mathbf{R}_I\end{bmatrix}. \tag{2.26}$$

where

$$\begin{aligned}\hat{\mathbf{u}} &\approx \Psi_1^R q_1^R+\Psi_2^R q_2^R+\cdots+\Psi_6^R q_6^R\\ &=\mathbf{\Psi}^R\mathbf{q}^R.\end{aligned} \tag{2.27}$$

in which $\Psi_i^R(i=1,2,\cdots,6)$ means the nodal vectors for the i th rigid body mode. By condensing out the fluid variables, we obtain the equation:

$$\left[-\omega^2\left(\mathbf{S}_M^R+\mathbf{S}_{MA}^R\right)+j\omega\mathbf{S}_{CW}^R+\mathbf{S}_K^R\right]\mathbf{q}^R=\mathbf{R}_W^R \tag{2.28}$$

for a rigid body motion analysis where super script R means rigid body motion and

$$\begin{aligned}
\mathbf{S}_M^R &= \mathbf{\Psi}^{R^{\mathrm{T}}}\mathbf{S}_M\mathbf{\Psi}^R && \text{: mass matrix,}\\
\mathbf{S}_{MA}^R &= \mathrm{Re}\left[\left(\mathbf{\Psi}^{R^{\mathrm{T}}}\mathbf{S}_D\right)\left(2\pi\mathbf{F}_M-\mathbf{F}_{Gn}\right)^{-1}\left(\mathbf{F}_G\mathbf{\Psi}^R\right)\right] && \text{: added mass matrix,}\\
\mathbf{S}_{CW}^R &= -\omega\times\mathrm{Im}\left[\left(\mathbf{\Psi}^{R^{\mathrm{T}}}\mathbf{S}_D\right)\left(2\pi\mathbf{F}_M-\mathbf{F}_{Gn}\right)^{-1}\left(\mathbf{F}_G\mathbf{\Psi}^R\right)\right] && \text{: radiated wave damping matrix,}\\
\mathbf{S}_K^R &= \mathbf{\Psi}^{R^{\mathrm{T}}}\left(\mathbf{S}_{HS}-\mathbf{S}_{HB}-\mathbf{S}_{HD}-\mathbf{S}_{HN}\right)\mathbf{\Psi}^R && \text{: hydrostatic stiffness matrix,}\\
\mathbf{R}_W^R &= j\omega\mathbf{\Psi}^{R^{\mathrm{T}}}\mathbf{S}_D\left(2\pi\mathbf{F}_M-\mathbf{F}_{Gn}\right)^{-1}\left(4\pi\mathbf{R}_I\right) && \text{: wave excitation forces vector.}
\end{aligned} \tag{2.29}$$

Equation (2.26) corresponds to conventional equation for rigid body motion analysis. Kim [7] presented detail derivation procedure and comparison of the direct coupling formulation and the conventional formulation. Numerical results presented by Kim show good agreement with results of WAMIT that is the most advanced software.

In this chapter, we derive the boundary integral equation and describe the conversion of continuous Equation (2.19) to discrete linear system of equation. This linear system of equation becomes ill-conditioned near the irregular frequencies [6], so solution near the irregular frequencies are erroneous. The bandwidth of polluted solution can be narrowed by discretizing the wet-surface finer, but it is not practical in aspect of computational cost. Thus, many researchers have developed the irregular frequency removal methods. We define the irregular frequency and review the existing methods briefly. Then, we suggest the effective procedure to remove the irregular frequency effect arising in numerical solution.

Chapter 3. Irregular Frequency

In this chapter, we first define the irregular frequency of the boundary integral equation we derived in previous chapter, and identify the location of the irregular frequencies for barge, circular cylinder. Secondly, we introduce the irregular frequency removal (IRR) methods that have been developed briefly and explain the removal principal of the extended boundary integral equation that is one of the IRR methods.

3.1 Definition of the Irregular Frequency

Equation (2.19) that represents the exterior Neumann problem presented in section 2.2.1 is known as possessing the irregular frequencies, and type of equation should be identified before defining the irregular frequencies. The most general type of linear integral equation is

$$h(x)g(x)+\lambda\int_{a} K(x,\xi)g(\xi)d\xi = f(x), \tag{3.1}$$

where the upper limit of the integral could be either variable or fixed [13]. $g(x)$ is the unknown function. $h(x)$ and $f(x)$ are known functions and $K(x,\xi)$ is the Kernel. λ is the nonzero parameter. Equation (2.19) has changed over to the equation:

$$\begin{aligned} 2\pi\phi(\mathbf{x})+\int_{S_B}\left[\{2\pi\phi(\xi)\}\left\{\frac{1}{2\pi}\frac{\partial G(\mathbf{x};\xi)}{\partial n(\xi)}\right\}\right]dS(\xi) \\ =\int_{S_B}\left[G(\mathbf{x};\xi)\frac{\partial\phi(\xi)}{\partial n(\xi)}\right]dS(\xi)+4\pi\phi_I(\mathbf{x}) \end{aligned} \quad \text{for } \mathbf{x} \text{ on } S_B \tag{3.2}$$

to identify the type of the integral equation. Equation (3.2) is the linear integral equation because Equation (3.2) corresponds with Equation (3.1) that is the general type of linear integral equation. To compare clearly, we note equations:

$$
\begin{aligned}
g(x) &= 2\pi\phi(\mathbf{x}) \\
h(x) &= 1 \\
f(x) &= \int_{S_B} \left[G(\mathbf{x};\boldsymbol{\xi}) \frac{\partial \phi(\boldsymbol{\xi})}{\partial n(\boldsymbol{\xi})} \right] dS(\boldsymbol{\xi}) + 4\pi\phi_I(\mathbf{x}). \\
K(x,\xi) &= \frac{1}{2\pi} \frac{\partial G(\mathbf{x};\boldsymbol{\xi})}{\partial n(\boldsymbol{\xi})} \\
\lambda &= 1
\end{aligned}
\tag{3.3}
$$

The upper limit of the integral is fixed and $h(x)$ is '1' and $f(x)$ is not zero. Therefore, the boundary integral equation (2.19) representing the boundary value problem presented in section 2.2.1 is the linear inhomogeneous Fredholm integral equation of the second kind.

It is well known that the occurrence of the irregular frequency is due to the existence and uniqueness of the integral equation, and the Fredholm's theorem describe the existence and uniqueness of the solution. Therefore, we briefly introduce the Fredholm's theorems. For more information, please refer the text book written by RAM [13].

3.1.1 Fredholm's Theorem

Fredholm's theorems for integral equations give the general solution of the linear inhomogeneous and homogenous Fredholm integral equations:

$$g(x) + \lambda \int_a^b K(x,\xi) g(\xi) d\xi = f(x), \tag{3.4}$$

$$g(x) + \lambda \int_a^b K(x,\xi) g(\xi) d\xi = 0, \tag{3.5}$$

and concerns the existence and uniqueness. Fredholm's theorems are closely related to linear algebra, and are usually dealt with the system of linear algebraic equations. Thus, we introduce the linear system of equations by confining discussion to one-dimensional integral, and discretizing the integral domain. We divide integral one-dimensional domain into n equal parts that has a length $h = (b-a)/n$ as shown in Figure 3.1 and then we obtain the approximate equation:

$$\int_a^b K(x,\xi) g(\xi) d\xi \approx h \sum_j^n K(x,\xi_j) g(\xi_j). \tag{3.6}$$

Equations (3.4) and (3.5) that integral is replaced using Equation (3.6) take the form

$$g(x)+\lambda h\sum_{j}^{n}K(x,\xi_j)g(\xi_j)\approx f(x), \tag{3.7}$$

$$g(x)+\lambda h\sum_{j}^{n}K(x,\xi_j)g(\xi_j)\approx 0\,. \tag{3.8}$$

Equations (3.7) and (3.8) are valid for n points on the integral domain, and these can be written as

$$g(x_i)+\lambda h\sum_{j}^{n}K(x_i,\xi_j)g(\xi_j)\approx f(x_i), \qquad \text{for } i = 1\sim n \tag{3.9}$$

$$g(x_i)+\lambda h\sum_{j}^{n}K(x_i,\xi_j)g(\xi_j)\approx 0. \qquad \text{for } i = 1\sim n \tag{3.10}$$

Figure 3.1. Discretization of one dimensional domain.

With expressions: $g(x_i)=g_i$, $f(x_i)=f_i$, and $K(x_i,\xi_j)=K_{ij}$, we obtain linear system of n equations with tensor representation:

$$g_i+\lambda h\sum_{j}^{n}K_{ij}g_j \approx f_i, \qquad \text{for } i = 1\sim n \tag{3.11}$$

$$g_i+\lambda h\sum_{j}^{n}K_{ij}g_j \approx 0. \qquad \text{for } i = 1\sim n \tag{3.12}$$

Equations (3.11) and (3.12) can be written in matrix representation:

$$[\mathbf{I}+\lambda\mathbf{K}]\mathbf{g}=\mathbf{f}\,, \tag{3.13}$$

$$[\mathbf{I}+\lambda\mathbf{K}]\mathbf{g}=\mathbf{0}\,, \tag{3.14}$$

where

$$\mathbf{I}=\begin{bmatrix}1 & 0 & \cdots & 0\\ 0 & 1 & \cdots & 0\\ \vdots & \vdots & \ddots & \vdots\\ 0 & 0 & \cdots & 1\end{bmatrix},\mathbf{K}=\begin{bmatrix}hK_{11} & hK_{12} & \cdots & hK_{1n}\\ hK_{21} & hK_{22} & \cdots & hK_{2n}\\ \vdots & \vdots & \ddots & \vdots\\ hK_{n1} & hK_{n2} & \cdots & hK_{nn}\end{bmatrix},\mathbf{g}=\begin{bmatrix}g_1\\ g_2\\ \vdots\\ g_n\end{bmatrix},\mathbf{f}=\begin{bmatrix}f_1\\ f_2\\ \vdots\\ f_n\end{bmatrix},\mathbf{0}=\begin{bmatrix}0\\ 0\\ \vdots\\ 0\end{bmatrix}. \tag{3.15}$$

The inhomogenous solution vector $\mathbf{g}_{inhomo}$ of Equation (3.13) contains the homogenous solution vector

$\mathbf{g}_{homo}$ of Equation (3.14), and judgment of the solution vector $\mathbf{g}$ of Equations (3.13) and (3.14) using linear algebra is well known. It depends on whether the resolvent determinant of the linear system of Equations (3.13) and (3.14):

$$D_n(\lambda) = \det\begin{bmatrix} 1+\lambda hK_{11} & \lambda hK_{12} & \cdots & \lambda hK_{1n} \\ \lambda hK_{21} & 1+\lambda hK_{22} & \cdots & \lambda hK_{2n} \\ \vdots & \vdots & \ddots & \vdots \\ \lambda hK_{n1} & \lambda hK_{n2} & \cdots & 1+\lambda hK_{nn} \end{bmatrix}, \tag{3.16}$$

where subscript n of D_n means the number of discretization, is zero or not.

In case of $D_n = 0$, parameter λ of Equations (3.13) and (3.14) is equal to one of eigenvalues of the eigenvalue problem:

$$\left[\mathbf{I} + \lambda_k^{eig}\mathbf{K}\right]\mathbf{g} = \mathbf{0}. \tag{3.17}$$

Therefore, equation (3.14) has at least one, and at most m, linearly independent solution, that is, $\mathbf{g}_{homo}$ is non-trivial solution. Each linearly independent solution is the eigenfunction of the eigenvalue problem (3.17).

Equation (3.13), meanwhile, possesses a solution when compatibility equation is satisfied. That equation is

$$rank[\mathbf{A}] = rank\left[\tilde{\mathbf{A}}\right], \tag{3.18}$$

where

$$\mathbf{A} = \begin{bmatrix} 1+\lambda hK_{11} & \lambda hK_{12} & \cdots & \lambda hK_{1n} \\ \lambda hK_{21} & 1+\lambda hK_{22} & \cdots & \lambda hK_{2n} \\ \vdots & \vdots & \ddots & \vdots \\ \lambda hK_{n1} & \lambda hK_{n2} & \cdots & 1+\lambda hK_{nn} \end{bmatrix},$$
$$\tilde{\mathbf{A}} = \left[\begin{array}{cccc|c} 1+\lambda hK_{11} & \lambda hK_{12} & \cdots & \lambda hK_{1n} & f_1 \\ \lambda hK_{21} & 1+\lambda hK_{22} & \cdots & \lambda hK_{2n} & f_2 \\ \vdots & \vdots & \ddots & \vdots & f_3 \\ \lambda hK_{n1} & \lambda hK_{n2} & \cdots & 1+\lambda hK_{nn} & f_4 \end{array}\right]. \tag{3.19}$$

However, even if $\mathbf{g}_{inhomo}$ exists, $\mathbf{g}_{inhomo}$ of Equation (3.13) is not a unique because it contains $\mathbf{g}_{homo}$ of Equation (3.14) that has infinite non-trivial solution.

In case of $D_n \neq 0$, it is evident that Equation (3.13) has a unique solution and Equation (3.14) has trivial solution. In other words, $\mathbf{g}_{homo}$ of Equation (3.14) is unique solution which is trivial solution and $\mathbf{g}_{inhomo}$ of Equation (3.13) is unique solution.

$\mathbf{g}_{inhomo}$ of Equation (3.13) contains $\mathbf{g}_{homo}$ of Equation (3.14), and the existence and uniqueness of $\mathbf{g}_{inhomo}$ depends on $\mathbf{g}_{homo}$ and $\mathbf{f}$. When $\mathbf{g}_{homo}$ is trivial solution, $\mathbf{g}_{inhomo}$ exists and is unique. However, $\mathbf{g}_{homo}$

is non-trivial solution, the existence of $\mathbf{g}_{inhomo}$ depends on $\mathbf{f}$, and even if it exists, it is not unique. In other words, the uniqueness of $\mathbf{g}_{inhomo}$ can be decided based on whether $\mathbf{g}_{homo}$ is trivial or non-trivial. Above statements are summarized in Tables 3.1 and 3.2.

Table 3.1. Existence and uniqueness of solution of homogenous linear system of equations.

$D_n(\lambda)$	$\mathbf{g}_{homo}$ of $[\mathbf{I}+\lambda\mathbf{K}]\mathbf{g}=\mathbf{0}$	
	Existence	Uniqueness
$D_n(\lambda)\neq 0$	O	Unique Solution (Trivial Solution)
$D_n(\lambda)=0$	O	Infinite Solutions (Non-Trivial Solutions)

Table 3.2. Existence and uniqueness of solution of inhomogenous linear system of equations.

$\mathbf{g}_{homo}$	$\mathbf{g}_{inhomo}$ of $[\mathbf{I}+\lambda\mathbf{K}]\mathbf{g}=\mathbf{f}$	
	Existence	Uniqueness
Trivial	O	Unique Solution
Non-Trivial	Depends on $\mathbf{f}$	Infinite Solutions (If exists)

The existence and uniqueness of solution of Fredholm integral equation correspond with the discrete linear system of equation obtained by discretization and approximation as written in first part of this section. In addition, there are two points should be considered before moving on to Fredholm's theorem. First, as n increase to infinity, $D_n(\lambda)$ becomes $D(\lambda)$ that is the resolvent determinant of Equations (3.4) and (3.5). Second, the compatibility equation that related to the existence of the $\mathbf{g}_{inhomo}$ when $\mathbf{g}_{homo}$ is non-trivial, differs from the discrete linear system of equation.

Fredholm's first and third theorems state the existence and the uniqueness of inhomogeneous Fredholm integral equation. Fredholm's second theorem describes the existence and uniqueness of homogenous Fredholm integral equation. Three theorems also give the solution of the series form.

The integral equation that we solve is the inhomogenous Fredholm integral equation, so Fredholm's first and third theorem should be considered. In case of $D_n \neq 0$, $\mathbf{g}_{inhomo}$ exists and is unique. However, in case of $D(\lambda)=0$, the existence of $\mathbf{g}_{inhomo}$ depends on whether the compatibility equation is satisfied or not. The compatibility equation is that the given function $f(x)$ is orthogonal to every solution of the adjoint homogenous equation:

$$p(x)+\lambda\int_a^b K^*(x,\xi)p(\xi)d\xi = 0, \tag{3.20}$$

that is

$$\int_a^b p(x)f(x)dx = 0, \tag{3.21}$$

where the superscript * means a complex conjugate. Even if $\mathbf{g}_{inhomo}$ exists, it is not unique because it contains $\mathbf{g}_{homo}$ that is non-trivial. Above statements are summarized in Table. 3.3.

Table 3.3 Existence and Uniqueness of Solution of Inhomogenous linear Fredholm equation of second kind.

g_{homo}	g_{inhomo} of $g(x)+\lambda\int_a^b K(x,\xi)g(\xi)d\xi = f(x)$		
	Theorem	Existence	Uniqueness
Unique Solution (Trivial Solution)	Fredholm's First	O	Unique Solution
Infinite Solutions (Non-Trivial Solutions)	Fredholm's Third	Depends on $f(x)$	Infinite Solutions (If exists)

3.1.2 Existence and Uniqueness of Solution of the Exterior Neumann Problem

Let's identify the existence and uniqueness of solution of equation (3.2). Equation (3.2) is the linear inhomogeneous Fredholm equation of the second kind, and corresponding homogeneous equation is

$$2\pi\phi(\mathbf{x})+\int_{S_B}\left[2\pi\phi(\xi)\left(\frac{1}{2\pi}\frac{\partial G(\mathbf{x};\xi)}{\partial n(\xi)}\right)\right]dS(\xi)=0, \qquad \text{for } \mathbf{x} \text{ on } S_B \qquad (3.22)$$

that has the kernel is the function of wave frequency. The homogenous solution of Equation (3.22) can be the trivial solution or the non-trivial solution, and is part of the inhomogenenous solution of Equation (3.2). Fredholm's third theorem state about the inhomogenous solution when homogenous solution is trivial and non-trivial.

Based on Fredholm's first theorem, Equation (3.2) has the unique solution when the homogenous solution is the trivial solution. According to Fredholm's third theorem, the compatibility Equation (3.21) should be satisfied in order that Equation (3.2) have a solution when homogenous solution is the non-trivial solution. By substituting integral domain, known function, and the non-trivial solution of the homogenous equation, the compatibility equation becomes

$$\int_{S_B}\varphi(\mathbf{x})\left\{\int_{S_B}G(\mathbf{x};\xi)\frac{\partial\phi(\xi)}{\partial n(\xi)}dS(\xi)+4\pi\phi_I(\mathbf{x})\right\}dx=0, \qquad (3.23)$$

where $\varphi(\mathbf{x})$ is the non-trivial solution of the homogenous adjoint equation:

$$2\pi\varphi(\mathbf{x})+\int_{S_B}\left[2\pi\varphi(\xi)\left(\frac{1}{2\pi}\frac{\partial G^*(\mathbf{x};\xi)}{\partial n(\xi)}\right)\right]dS(\xi)=0, \qquad \text{for } \mathbf{x} \text{ on } S_B \qquad (3.24)$$

corresponding to Equation (3.2). Proof of Equation (3.23) can be shown by introducing the adjoint homogenous equation and the interior Dirichlet problem considering potential $\hat{\phi}$ that satisfies the Laplace equation, the free-surface boundary condition on S_I, and homogeneous Dirichlet boundary condtion on S_B. Detail proof is written in section 3.1.4. However, even if Equation (3.23) is satisfied, Equation (3.2) has infinite solution because Equation (2.19) cannot be determined uniquely, that is, the solution of inhomogenous Equation (3.2) contains the solution of homogeneous equation that has at least one linearly independent solution that makes infinite cases of homogeneous solution. This non-trivial solution of Equation (3.22) is a solution of interior Dirichlet problem. We present how Equation (3.22) and the interior Dirichlet problem are connected in section 3.1.4.

In summary, the solution of Equation (3.2) always exists, and is unique only when the solution of Equation (3.22) is the trivial solution. Therefore, the irregular frequency is the wave frequency that make the solution of Equation (3.22) the non-trivial solution.

3.1.3 Interior Dirichlet Problem

In this section, we show that Equation (3.22) is related to the interior Dirichlet problem which is fictitious and has nothing to with physical sloshing of interior domain. Interior problem domain is shown in Figure 3.2.

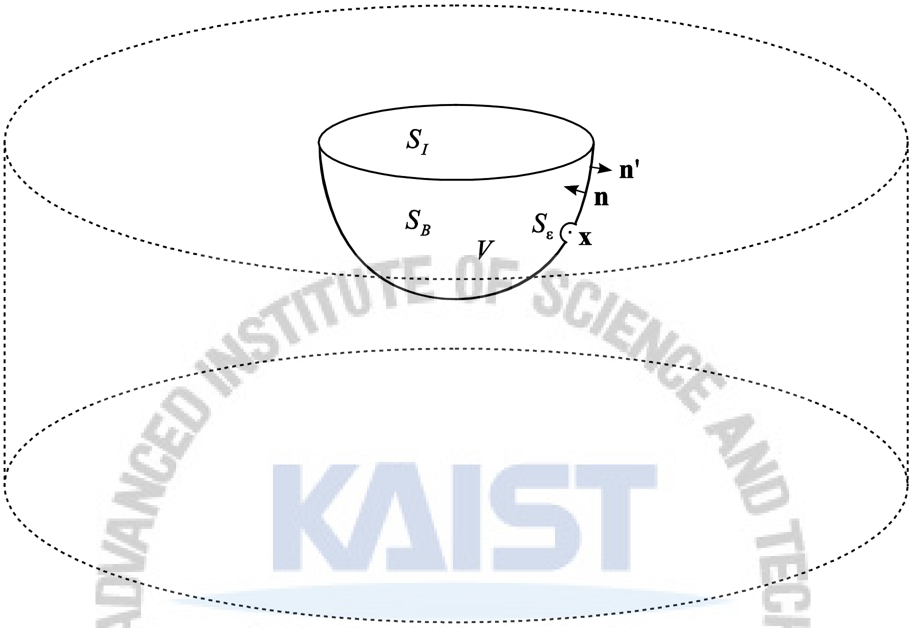

Figure 3.2. Domain of Interior Dirichlet Problem.

Let's apply Equation (2.14) for interior potential $\hat{\phi}$ that satisfies the free surface boundary condition and G in fluid domain V_I surrounded by surfaces: S_B and S_I, and then we obtain

$$2\pi\hat{\phi}(\mathbf{x})+\int_{S_B+S_I}\left[\hat{\phi}(\xi)\frac{\partial G(\mathbf{x};\xi)}{\partial n'(\xi)}-G(\mathbf{x};\xi)\frac{\partial\hat{\phi}(\xi)}{\partial n'(\xi)}\right]dS(\xi)=0. \qquad \text{for } \mathbf{x} \text{ on } S_B \qquad (3.25)$$

Because G has the same boundary condition on S_I with $\hat{\phi}$, we get

$$2\pi\hat{\phi}(\mathbf{x})-\int_{S_B}\left[\hat{\phi}(\xi)\frac{\partial G(\mathbf{x};\xi)}{\partial n(\xi)}\right]dS(\xi)=-\int_{S_B}\left[G(\mathbf{x};\xi)\frac{\partial\hat{\phi}(\xi)}{\partial n(\xi)}\right]dS(\xi). \qquad \text{for } \mathbf{x} \text{ on } S_B \qquad (3.26)$$

The differentiation of Equation (3.26) with respect to the normal vector at field point $\mathbf{x}$ on S_B is

$$\begin{aligned}2\pi\frac{\partial\hat{\phi}(\mathbf{x})}{\partial n(\mathbf{x})}-\frac{\partial}{\partial n(\mathbf{x})}\int_{S_B}\left[\hat{\phi}(\xi)\frac{\partial G(\mathbf{x};\xi)}{\partial n(\xi)}\right]dS(\xi)=\\-\int_{S_B}\left[\frac{\partial G(\mathbf{x};\xi)}{\partial n(\mathbf{x})}\frac{\partial\hat{\phi}(\xi)}{\partial n(\xi)}\right]dS(\xi).\end{aligned} \qquad \text{for } \mathbf{x} \text{ on } S_B \qquad (3.27)$$

One should note that whereas the sign of parameter λ in Equation (2.19) is positive, the sign of parameter λ in Equation (3.25) is negative, because the direction of $\mathbf{n}$ of V_F and the direction of $\mathbf{n}'$ of V_I are opposite. Now, let's consider the Dirichlet and Neumann boundary conditions on S_B. When $\partial\hat{\phi}/\partial n = 0$, the interior potential means the physical sloshing and Equation (3.26) becomes

$$2\pi\hat{\phi}(\mathbf{x}) - \int_{S_B}\left[\hat{\phi}(\xi)\frac{\partial G(\mathbf{x};\xi)}{\partial n(\xi)}\right]dS(\xi) = 0\,, \qquad \text{for } \mathbf{x} \text{ on } S_B \tag{3.28}$$

so it has nothing to do with Equation (3.2). When $\hat{\phi} = 0$, the interior potential does not have the physical relationship with Neumann exterior boundary value problem that presented in chapter 2, and Equation (3.27) becomes

$$\cdot\, 2\pi\frac{\partial\hat{\phi}(\mathbf{x})}{\partial n(\mathbf{x})} + \int_{S_B}\left[\left\{2\pi\frac{\partial\hat{\phi}(\xi)}{\partial n(\xi)}\right\}\frac{1}{2\pi}\frac{\partial G(\mathbf{x};\xi)}{\partial n(\mathbf{x})}\right]dS(\xi) = 0. \qquad \text{for } \mathbf{x} \text{ on } S_B \tag{3.29}$$

Kernel, parameter, and integral surface of Equation (3.29) and Equation (3.2) are equal, so the relation between the exterior Neumann problem and the interior Dirichlet problem is presented.

3.1.4 Adjoint Homogenous Equation

In this section, we show that the compatibility equation that assures the existence of solution of Equation (3.2) when homogeneous solution is non-trivial is valid. To prove that, we first compare the adjoint homogeneous equation of the interior Dirichlet problem and the exterior Neumann problem that are represented in the integral Equations (3.24) and (3.2) respectively. The adjoint homogenous form of Equation (3.2) is

$$2\pi\varphi(\mathbf{x}) + \int_{S_B}\left[\{2\pi\varphi(\xi)\}\left\{\frac{1}{2\pi}\frac{\partial G^*(\mathbf{x};\xi)}{\partial n(\xi)}\right\}\right]dS(\xi) = 0, \qquad \text{for } \mathbf{x} \text{ on } S_B \tag{3.30}$$

and the adjoint homogenous form of Equation (3.24) is

$$2\pi\frac{\partial\hat{\varphi}(\mathbf{x})}{\partial n(\mathbf{x})} + \int_{S_B}\left[\left\{2\pi\frac{\partial\hat{\varphi}(\xi)}{\partial n(\xi)}\right\}\frac{1}{2\pi}\frac{\partial G^*(\mathbf{x};\xi)}{\partial n(\mathbf{x})}\right]dS(\xi) = 0. \qquad \text{for } \mathbf{x} \text{ on } S_B \tag{3.31}$$

The identity

$$\varphi(\mathbf{x}) = \frac{\partial\hat{\varphi}(\mathbf{x})}{\partial n(\mathbf{x})} \tag{3.32}$$

is established by comparison Equations (3.30) and (3.31).

Secondly, we consider the adjoint homogenous form of Equation (3.26):

$$2\pi\hat{\varphi}(\mathbf{x}) - \int_{S_B}\left[\hat{\varphi}(\xi)\frac{\partial G(\mathbf{x};\xi)}{\partial n(\xi)}\right]dS(\xi) = -\int_{S_B}\left[G(\mathbf{x};\xi)\frac{\partial\hat{\varphi}(\xi)}{\partial n(\xi)}\right]dS(\xi), \qquad \text{for } \mathbf{x} \text{ on } S_B \tag{3.33}$$

and adopt the boundary condition on $\hat{\varphi} = 0$ on S_B Equation (3.33), and get

$$\int_{S_B}\left[G(\mathbf{x};\xi)\frac{\partial\hat{\varphi}(\xi)}{\partial n(\xi)}\right]dS(\xi) = 0. \qquad \text{for } \mathbf{x} \text{ on } S_B \tag{3.34}$$

Thirdly, we apply Equation (2.14) for incident wave potential ϕ_I and adjoint interior potential $\hat{\varphi}$ in fluid domain V_I surrounded by surfaces: S_B, and S_I. Incident wave potential satisfies the free-surface boundary condition on S_I and adjoint interior potential satisfies the free-surface boundary condition on S_I and the homogeneous Dirichlet condition on S_B. We obtain

$$\int_{S_B}\left[\phi_I(\mathbf{x})\frac{\partial\hat{\varphi}(\mathbf{x})}{\partial n(\mathbf{x})}\right]dS(\xi) = \int_{S_B}\left[\hat{\varphi}(\mathbf{x})\frac{\partial\phi_I(\mathbf{x})}{\partial n(\mathbf{x})}\right]dS(\xi) = 0. \qquad \text{for } \mathbf{x} \text{ on } S_B \tag{3.35}$$

Finally, we can prove Equation (3.23). By substituting Equation (3.32) into Equation (3.23), we obtain

$$\int_{S_B}\frac{\partial\hat{\varphi}(\mathbf{x})}{\partial n(\mathbf{x})}\left\{\int_{S_B}G(\mathbf{x};\xi)\frac{\partial\phi(\xi)}{\partial n(\xi)}dS(\xi)\right\}dS(\mathbf{x}) + \int_{S_B}\frac{\partial\hat{\varphi}(\mathbf{x})}{\partial n(\mathbf{x})}\times 4\pi\phi_I(\mathbf{x})dS(\mathbf{x}) = 0, \tag{3.36}$$

and the first term of Equation (3.36) becomes

$$\int_{S_B}\frac{\partial\phi(\xi)}{\partial n(\xi)}\left\{\int_{S_B}G(\mathbf{x};\xi)\frac{\partial\hat{\varphi}(\mathbf{x})}{\partial n(\mathbf{x})}dS(\mathbf{x})\right\}dS(\xi) = 0, \tag{3.37}$$

by changing order of integral and substituting Equation (3.34). The second term of Equation (3.36) becomes

$$4\pi\int_{S_B}\frac{\partial\hat{\varphi}(\mathbf{x})}{\partial n(\mathbf{x})}\phi_I(\mathbf{x})dS(\mathbf{x}) = 4\pi\int_{S_B}\hat{\varphi}(\mathbf{x})\frac{\partial\phi_I(\mathbf{x})}{\partial n(\mathbf{x})}dS(\xi) = 0 \tag{3.38}$$

by using Equation (3.35) and boundary condition $\hat{\varphi} = 0$.

3.1.5 Occurrence of the Irregular Frequency

As discussed in the several previous sections, Equation (3.2) representing the exterior Neumann problem always has a solution and is unique only if solution of the interior Dirichlet problem of which solution vary according to wave frequency is trivial. Therefore, when a solution of the Dirichlet problem is non-trivial, a solution of the exterior Neumann problem is not a unique, and corresponding wave frequencies that make a solution of the exterior Neumann problem not unique are called the irregular frequencies.

In other words, the interior Dirichlet problem could have the trivial or non-trivial solution depending on a wave frequency. Therefore, if we know the analytical solution of the interior Dirichlet problem, it is possible to distinguish the irregular frequencies. However, it is difficult to solve the interior Dirichlet problem analytically except simple geometry problem like barge, and circular cylinder. Accordingly, it is not possible to predict the irregular frequency in most cases.

3.2 Location of the Irregular Frequency

In this section, we present the location of the irregular frequencies for barge and circular cylinder by solving the interior Dirichlet problem analytically.

3.2.1 Barge

We assumed a harmonic time dependence, so we define the velocity potential as ${}^{\tau}\varphi^B = \mathrm{Re}\left[\varphi^B e^{j\omega t}\right]$. For a barge with the length L, the breadth B, and the draft T as shown in Fig. 3.3, the velocity potential φ^B satisfies the Laplace equation:

$$\nabla^2 \varphi^B = \frac{\partial^2 \varphi^B}{\partial x_1^2} + \frac{\partial^2 \varphi^B}{\partial x_2^2} + \frac{\partial^2 \varphi^B}{\partial x_3^2} = 0, \tag{3.39}$$

the linearized free-surface boundary condition:

$$\frac{\partial \varphi^B (x_1, x_2, T)}{\partial x_3} = \frac{\omega^2}{g} \varphi^B (x_1, x_2, T), \qquad \text{on } S_I \tag{3.40}$$

the homogeneous Dirichlet condition:

$$\varphi^B (0, x_2, x_3) = \varphi^B (L, x_2, x_3) = \varphi^B (x_1, 0, x_3) = \varphi^B (x_1, B, x_3) = 0, \qquad \text{on } S_B \tag{3.41}$$

$$\varphi^B (x_1, x_2, 0) = 0. \qquad \text{on } S_B \tag{3.42}$$

By assuming the velocity potential as

$$\varphi^B (x_1, x_2, x_3) = \sum_{n=1}^{\infty} \sum_{m=1}^{\infty} b_{nm}(x_3) \sin\left(\frac{n\pi x_1}{L}\right) \sin\left(\frac{m\pi x_2}{B}\right) \tag{3.43}$$

The series form of the velocity potential (3.43) satisfies the boundary condition (3.42), and its double derivatives with respect to x_1, and x_2 are

$$\frac{\partial\varphi^B(x_1,x_2,x_3)}{\partial x_1^2} = -\sum_{n=1}^{\infty}\sum_{m=1}^{\infty}\left(\frac{n\pi}{L}\right)^2 b_{nm}(x_3)\sin\left(\frac{n\pi\, x_1}{L}\right)\sin\left(\frac{m\pi\, x_2}{B}\right) \tag{3.44}$$

$$\frac{\partial\varphi^B(x_1,x_2,x_3)}{\partial x_2^2} = -\sum_{n=1}^{\infty}\sum_{m=1}^{\infty}\left(\frac{m\pi}{B}\right)^2 b_{nm}(x_3)\sin\left(\frac{n\pi\, x_1}{L}\right)\sin\left(\frac{m\pi\, x_2}{B}\right) \tag{3.45}$$

By substituting Equations (3.44) and (3.45) into the Laplace equation, Equation (3.40) becomes

$$\begin{aligned}&\sum_{n=1}^{\infty}\sum_{m=1}^{\infty}\frac{\partial^2 b_{nm}(x_3)}{\partial x_3^2}\sin\left(\frac{n\pi\, x_1}{L}\right)\sin\left(\frac{m\pi\, x_2}{B}\right)\\ &-\sum_{n=1}^{\infty}\sum_{m=1}^{\infty}\left[\left(\frac{n\pi}{L}\right)^2+\left(\frac{m\pi}{B}\right)^2\right]b_{nm}(x_3)\sin\left(\frac{n\pi\, x_1}{L}\right)\sin\left(\frac{m\pi\, x_2}{B}\right)=0.\end{aligned} \tag{3.46}$$

If we introduce the parameter: $\gamma = \left[\left(\frac{n\pi}{L}\right)^2+\left(\frac{m\pi}{B}\right)^2\right]^{1/2}$, then we get

$$\frac{\partial^2 b_{nm}(x_3)}{\partial x_3^2} - \gamma^2 b_{nm}(x_3) = 0\,. \tag{3.47}$$

The general solution of Equation (3.47) is

$$b_{nm}(x_3) = A_{nm}e^{\gamma x_3} + C_{nm}e^{-\gamma x_3}\,, \tag{3.48}$$

where A_{nm} and C_{nm} are the arbitrary constants should be determined by adopting the boundary condition. Now, we find the relation that is $A_{nm} = C_{nm}$ by applying the boundary condition (3.42), and we obtain

$$\varphi^B(x_1,x_2,x_3) = 2A_{nm}\sinh(\gamma\, x_3)\sin\left(\frac{n\pi\, x_1}{L}\right)\sin\left(\frac{m\pi\, x_2}{B}\right) \qquad \text{for}\quad n,m=1,2,\cdots \tag{3.49}$$

Finally with the linearized free-surface boundary condition, we have the equation:

$$\omega_{irr}^B = \sqrt{g\gamma\coth(\gamma T)} \tag{3.50}$$

that represents the irregular frequencies of the barge problem [14].

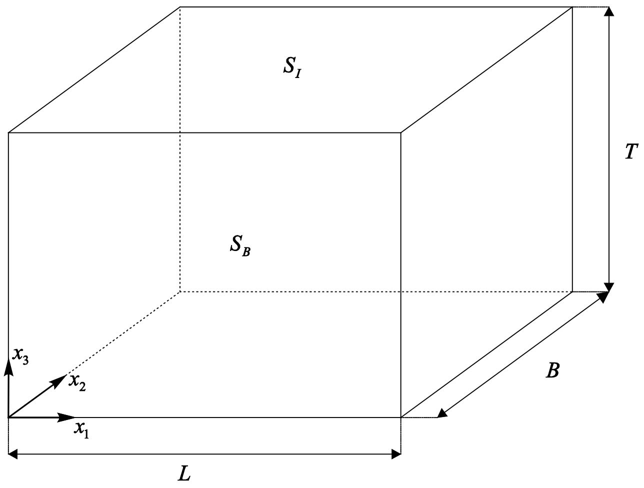

Figure 3.3. Schema of the Interior Dirichlet Problem (Barge).

3.2.2 Circular Cylinder

We define the velocity potential as ${}^{\tau}\varphi^C = \mathrm{Re}\left[\varphi^C e^{j\omega t}\right]$ by assuming a time harmonic dependence. For a circular cylinder the radius R, and the draft T as shown in Fig. 3.4, the velocity potential φ^C satisfies the Laplace equation:

$$\nabla^2\varphi^C = \frac{1}{r}\frac{\partial}{\partial r}\left(r\frac{\partial\varphi^C}{\partial r}\right) + \frac{1}{r^2}\frac{\partial^2\varphi^C}{\partial r^2} + \frac{\partial^2\varphi^C}{\partial z} = 0, \tag{3.51}$$

the linearized free-surface boundary condition:

$$\frac{\partial\varphi^C(r,\theta,0)}{\partial z} = \frac{\omega^2}{g}\varphi^C(r,\theta,0), \qquad \text{on } S_I \tag{3.52}$$

the homogeneous Dirichlet condition:

$$\varphi^C(R,\theta,z) = 0, \qquad \text{on } S_B \tag{3.53}$$

$$\varphi^C(r,\theta,-T) = 0. \qquad \text{on } S_B \tag{3.54}$$

By assuming the velocity potential as

$$\varphi^C(r,\theta,z) = \sum_{m=1}^{\infty}\sum_{n=1}^{\infty} A_{mn}\left[\sinh\{n(z+T)\}\right] \times \{\cos(m\theta) + \sin(m\theta)\} J_m(nr), \tag{3.55}$$

where J_m is the Bessel function of order m. The series form of the velocity potential (3.55) satisfies the boundary condition (3.54). To satisfy the boundary condition (3.53), we define n that satisfies $J_m(nR) = 0$. We rewrite Equation (3.55) as in the field of

$$\varphi^C(r,\theta,z)=\sum_{m=1}^{\infty}A_m[\sinh\{n(z+T)\}]\times\{\cos(m\theta)+\sin(m\theta)\}J_m(nR). \tag{3.56}$$

Finally with the linearized free-surface boundary condition, we have the equation:

$$\omega_{irr}^C=\sqrt{g\frac{n}{\tanh(nT)}}. \tag{3.57}$$

that represents the irregular frequencies of the circular cylinder problem.

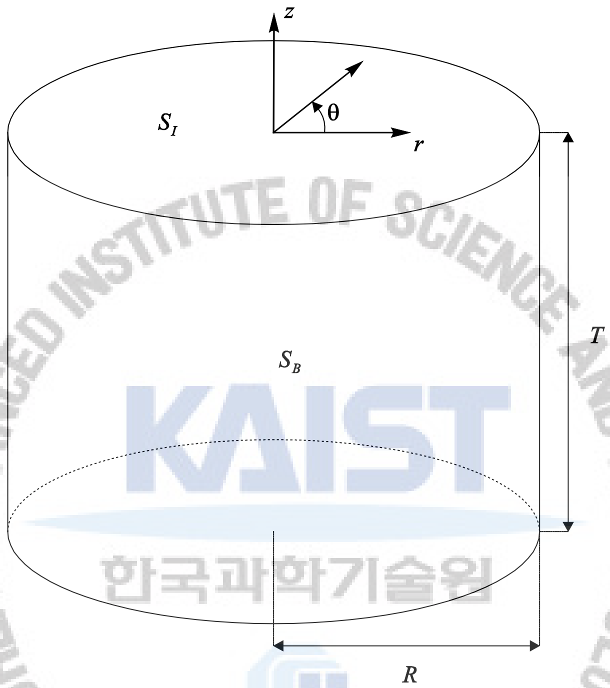

Figure 3.4 Schema of the Interior Dirichlet Problem (Circular Cylinder).

3.3 Irregular Frequency Removal Method

Since the existence of the irregular frequencies was reported by Lamb [2], several IRR methods have been suggested in the field of acoustics and water wave problems. These methods can be classified into two categories [4]:

(1) Modification of the integral operator

(2) Modification of the domain of the integral operator.

Representative methods in the first category are the Modified Green function method [15], the Null-field equation method [16], and the Modified integral-equation method [6]. In the second category, there are two typical methods: the Combined boundary integral equation(CBIE) method, and the Extended boundary integral equation(EBIE) method, and the principle is the same [4, 17]. The ease of implementation, the computational cost aspect, and general applicability should be considered when choosing one of methods. Methods in the first category increase relatively small computational cost and are applicable for three-dimensional body, but not suitable for arbitrary shape body. Meanwhile, the CBIE method and the EBIE are applicable for three-dimensional structure, and the EBIE method are suitable for a structure of arbitrary shape. However, the increment of computational cost of the EBIE method is relatively larger than methods in the first category. Detailed contents are described in related papers and we summarize that briefly in Table 3.4. In Table 3.4, the quantitative comparison is presented because comparison of cost increment is related to several factors, and △ means that it is difficult to apply to structure of arbitrary shape because particular factors such as field point, arbitrary constant are involved.

Table 3.4. Comparison of irregular frequency removal methods.

	Three Dimension	Arbitrary Shape	Cost Increment
Modified Green-function Method	Available	△	Low
Null-field equation Method	Available	Not Available	Low
Modified Integral-equation Method	Available	△	Mid
CBIE Method	Available	△	Low
EBIE Method	Available	Available	High

Although the EBIE method increases the computational cost considerably, it is applicable to the three dimensional floating structure of arbitrary shape. Therefore, we use the EBIE method for procedure to remove the irregular frequency effect in numerical analysis presented in the chapter 4. The principle of the CBIE and

EBIE methods is suppressing the non-trivial solution of the interior Dirichlet problem by imposing homogenous Dirichlet boundary condition on S_I. Through the EBIE method, Equation (2.19) is transformed into

$$\begin{aligned} 2\pi\phi^B(\mathbf{x}) &+ \int_{S_B}\left[\phi^B(\xi)\frac{\partial G(\mathbf{x};\xi)}{\partial n(\xi)}\right]dS(\xi) \\ &+ \int_{S_I}\left[\phi^I(\xi)\frac{\partial G(\mathbf{x};\xi)}{\partial n(\xi)}\right]dS(\xi) \\ &= \int_{S_B}\left[G(\mathbf{x};\xi)\frac{\partial \phi^B(\xi)}{\partial n(\xi)}\right]dS(\xi) + 4\pi\phi_I(\mathbf{x}), \end{aligned} \qquad \text{for } \mathbf{x} \text{ on } S_B \tag{3.58}$$

$$\begin{aligned} -4\pi\phi^I(\mathbf{x}) &+ \int_{S_B}\left[\phi^B(\xi)\frac{\partial G(\mathbf{x};\xi)}{\partial n(\xi)}\right]dS(\xi) \\ &+ \int_{S_I}\left[\phi^I(\xi)\frac{\partial G(\mathbf{x};\xi)}{\partial n(\xi)}\right]dS(\xi) \\ &= \int_{S_B}\left[G(\mathbf{x};\xi)\frac{\partial \phi^B(\xi)}{\partial n(\xi)}\right]dS(\xi) + 4\pi\phi_I(\mathbf{x}) \end{aligned} \qquad \text{for } \mathbf{x} \text{ on } S_I \tag{3.59}$$

where ϕ^B and ϕ^I are the velocity potentials on S_B and S_I, respectively. For detail procedure, please refer the paper written by Lee [17]. We construct the discrete linear system of equation through variational formulation, and boundary element discretization, then

$$\begin{bmatrix} -\omega^2\mathbf{S}_M + \mathbf{S}_K + \mathbf{S}_{KN} - \mathbf{S}_{HD} - \mathbf{S}_{HN} & -j\omega\mathbf{S}_D \\ j\omega\mathbf{F}_G^{Total} & \mathbf{F}_M^{Total} - \mathbf{F}_{Gn}^{Total} \end{bmatrix}\begin{bmatrix} \hat{\mathbf{u}} \\ \hat{\boldsymbol{\varphi}}^{Total} \end{bmatrix} = \begin{bmatrix} 0 \\ 4\pi\mathbf{R}_I^{Total} \end{bmatrix} \tag{3.60}$$

where

$$2\pi\int_{S_B}\phi(\mathbf{x})\bar{\phi}(\mathbf{x})dS(\mathbf{x}) = \hat{\bar{\boldsymbol{\varphi}}}^{Total\,\mathrm{T}}\left[2\pi\mathbf{F}_M^B\right]\hat{\boldsymbol{\varphi}}^{Total}, \tag{3.61a}$$

$$-4\pi\int_{S_I}\phi(\mathbf{x})\bar{\phi}(\mathbf{x})dS(\mathbf{x}) = \hat{\bar{\boldsymbol{\varphi}}}^{Total\,\mathrm{T}}\left[-4\pi\mathbf{F}_M^I\right]\hat{\boldsymbol{\varphi}}^{Total}, \tag{3.61b}$$

$$\int_{S_B}\int_{S_B}\left[\phi(\xi)\frac{\partial G(\mathbf{x};\xi)}{\partial n(\xi)}\right]dS(\xi)\bar{\phi}(\mathbf{x})dS(\mathbf{x}) = \hat{\bar{\boldsymbol{\varphi}}}^{Total\,\mathrm{T}}\left[\mathbf{F}_{Gn}^{B,B}\right]\hat{\boldsymbol{\varphi}}^{Total}, \tag{3.61c}$$

$$\int_{S_B}\int_{S_I}\left[\phi(\xi)\frac{\partial G(\mathbf{x};\xi)}{\partial n(\xi)}\right]dS(\xi)\bar{\phi}(\mathbf{x})dS(\mathbf{x}) = \hat{\bar{\boldsymbol{\varphi}}}^{Total\,\mathrm{T}}\left[\mathbf{F}_{Gn}^{B,I}\right]\hat{\boldsymbol{\varphi}}^{Total}, \tag{3.61d}$$

$$\int_{S_I}\int_{S_B}\left[\phi(\xi)\frac{\partial G(\mathbf{x};\xi)}{\partial n(\xi)}\right]dS(\xi)\bar{\phi}(\mathbf{x})dS(\mathbf{x}) = \hat{\bar{\boldsymbol{\varphi}}}^{Total\,\mathrm{T}}\left[\mathbf{F}_{Gn}^{I,B}\right]\hat{\boldsymbol{\varphi}}^{Total}, \tag{3.61e}$$

$$\int_{S_I}\int_{S_I}\left[\phi(\xi)\frac{\partial G(\mathbf{x};\xi)}{\partial n(\xi)}\right]dS(\xi)\overline{\phi}(\mathbf{x})dS(\mathbf{x})=\hat{\bar{\boldsymbol{\varphi}}}^{Total^{\mathrm{T}}}\left[\mathbf{F}_{Gn}^{I,I}\right]\hat{\boldsymbol{\varphi}}^{Total}, \tag{3.61f}$$

$$j\omega\int_{S_B}\int_{S_B}\left[G(\mathbf{x};\xi)u_i(\xi)n_i(\xi)\right]dS(\xi)\overline{\phi}(\mathbf{x})dS(\mathbf{x})=\hat{\bar{\boldsymbol{\varphi}}}^{Total^{\mathrm{T}}}\left[j\omega\mathbf{F}_G^B\right]\hat{\mathbf{u}}, \tag{3.61g}$$

$$j\omega\int_{S_I}\int_{S_B}\left[G(\mathbf{x};\xi)u_i(\xi)n_i(\xi)\right]dS(\xi)\overline{\phi}(\mathbf{x})dS(\mathbf{x})=\hat{\bar{\boldsymbol{\varphi}}}^{Total^{\mathrm{T}}}\left[j\omega\mathbf{F}_G^I\right]\hat{\mathbf{u}}, \tag{3.61h}$$

$$\int_{S_B}4\pi\phi_I(\mathbf{x})\overline{\phi}(\mathbf{x})dS(\mathbf{x})=\hat{\bar{\boldsymbol{\varphi}}}^{Total^{\mathrm{T}}}\left[4\pi\mathbf{R}_I^B\right], \tag{3.61i}$$

$$\int_{S_I}4\pi\phi_I(\mathbf{x})\overline{\phi}(\mathbf{x})dS(\mathbf{x})=\hat{\bar{\boldsymbol{\varphi}}}^{Total^{\mathrm{T}}}\left[4\pi\mathbf{R}_I^I\right], \tag{3.61j}$$

$$\hat{\boldsymbol{\varphi}}^{Total}=\hat{\boldsymbol{\varphi}}^B+\hat{\boldsymbol{\varphi}}^I,\quad \mathbf{F}_G^{Total}=\mathbf{F}_G^B+\mathbf{F}_G^I,\quad \mathbf{F}_M^{Total}=2\pi\mathbf{F}_M^B-4\pi\mathbf{F}_M^I, \tag{3.61k}$$

$$\mathbf{F}_{Gn}^{Total}=\mathbf{F}_{Gn}^{B,B}+\mathbf{F}_{Gn}^{B,I}+\mathbf{F}_{Gn}^{I,B}+\mathbf{F}_{Gn}^{I,I},\quad \mathbf{R}_I^{Total}=\mathbf{R}_I^B+\mathbf{R}_I^I, \tag{3.61l}$$

for flexible floating body analysis. In the aforementioned expressions, $\hat{\boldsymbol{\varphi}}^B$ and $\hat{\boldsymbol{\varphi}}^I$ are the nodal velocity potential vectors on S_B and S_I, respectively. By expressing the displacement field by the six degrees of freedom, and condensing out the fluid variables, we obtain the following equation:

$$\left[-\omega^2\left(\mathbf{S}_M^R+\mathbf{S}_{MA}^R\right)+j\omega\mathbf{S}_{CW}^R+\mathbf{S}_K^R\right]\mathbf{q}^R=\mathbf{R}_W^R \tag{3.62}$$

of which mass and hydrostatic stiffness matrix are equal to those of equation (3.37). Added mass, radiated wave damping matrices, and wave excitation force vector are

$$\begin{aligned}
\mathbf{S}_{MA}^R&=\mathrm{Re}\left[\left(\boldsymbol{\Psi}^{R^{\mathrm{T}}}\mathbf{S}_D\right)\left(2\pi\mathbf{F}_M^{Total}-\mathbf{F}_{Gn}^{Total}\right)^{-1}\left(\mathbf{F}_G^{Total}\boldsymbol{\Psi}^R\right)\right],\\
\mathbf{S}_{CW}^R&=-\omega\times\mathrm{Im}\left[\left(\boldsymbol{\Psi}^{R^{\mathrm{T}}}\mathbf{S}_D\right)\left(2\pi\mathbf{F}_M^{Total}-\mathbf{F}_{Gn}^{Total}\right)^{-1}\left(\mathbf{F}_G^{Total}\boldsymbol{\Psi}^R\right)\right],\\
\mathbf{R}_W^R&=j\omega\boldsymbol{\Psi}^{R^{\mathrm{T}}}\mathbf{S}_D\left(2\pi\mathbf{F}_M^{Total}-\mathbf{F}_{Gn}^{Total}\right)^{-1}\left(4\pi\mathbf{R}_I^{Total}\right),
\end{aligned} \tag{3.63}$$

respectively.

Chapter 4. Cost Reduction Procedure for the Irregular Frequency Removal Method

The EBIE method is applicable to the three dimensional floating structure of arbitrary shape as mentioned in the previous chapter, but it increases the computational cost, Increment of the computational cost depends on the degree of freedom on the interior free-surface, because the EBIE method include the interior free-surface as part of domain. The degree of freedom on the interior free-surface vary depending on type of and floating structure. Here we present representative two examples: ship-shaped offshore unit, and ISSC tension-leg platform(TLP). Numerical hydrodynamic analyses are conducted under equivalent computational condition by WAMIT in frequency range from 0.2 ~ 1.5 rad/s and constant panel method [18] is used. The discretization of the ship-shaped offshore unit and ISSC TLP are shown in Figures 4.1 and 4.2. Table 4.1 summarize the degree of freedom on the wet surface and the internal free-surface, the computational time of original boundary integral equation(OBIE) method and extended boundary integral equation(EBIE) method.

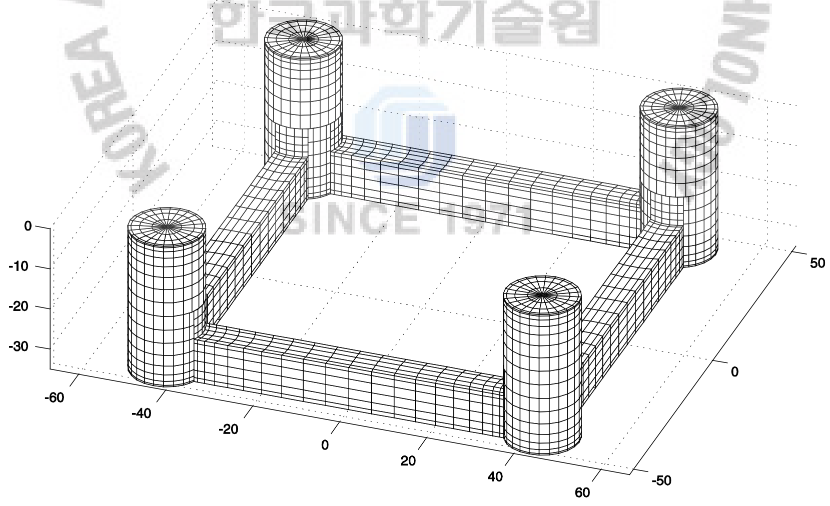

Figure 4.1. Discretization of the wet surface of ISSC TLP and the interior free-surface.

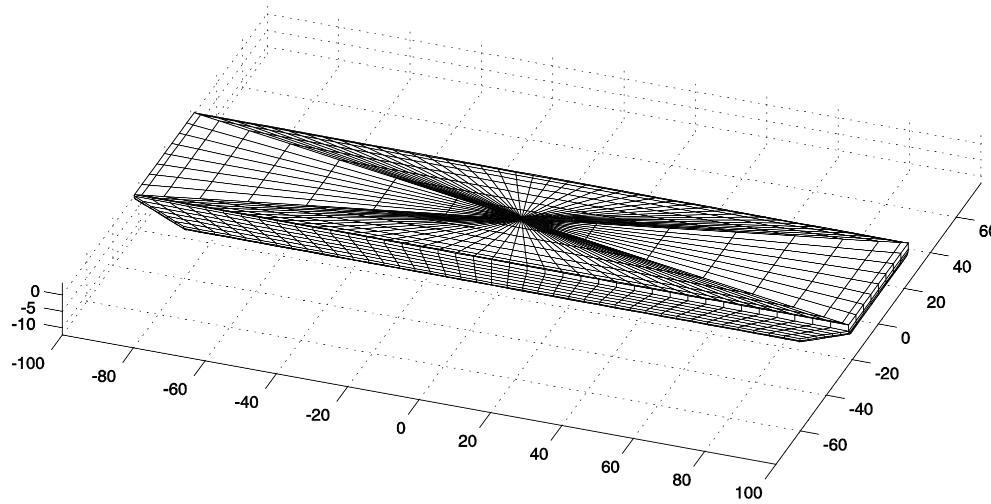

Figure 4.2. Discretization of the wet surface of ship-shaped offshore unit and the interior free-surface.

Table 4.1. Analysis condition and computational time of ship-shaped offshore unit and ISS TLP.

Ship-shaped offshore unit						ISSC TLP					
Degree of freedom			Computational Time			Degree of freedom			Computational Time		
S_B	S_I	S_I/S_B [%]	OBIE [s]	EBIE [s]	Increment [%]	S_B	S_I	S_I/S_B [%]	OBIE [s]	EBIE [s]	Increment [%]
1352	768	56.8	917	2365	157.9	4048	384	9.4	3171	6458	103.7

The computational cost of ship-shaped offshore unit and ISSC TLP increased 350.5% and 145.5% respectively. In this chapter, we present the procedure to reduce increment of the computational cost due to the EBIE method. The key concept of the cost reduction procedure for the IRR method is applying the EBIE method selectively. As shown in Figure 4.3, the numerical error due to the irregular frequencies appears over a substantial frequency band around the irregular frequencies. Therefore, the total computational cost can be reduced by applying the EBIE method only for discrete wave frequencies in “polluted” frequency band.

In this chapter, we first compare the numerical analysis procedure of OBIE and EBIE in terms of the computational cost. Second, we present the criterion that would be used to detect wave frequencies that are in “polluted” frequency band. Then, we finally propose the cost reduction procedure for the IRR method and examine feasibility and limitation of this procedure.

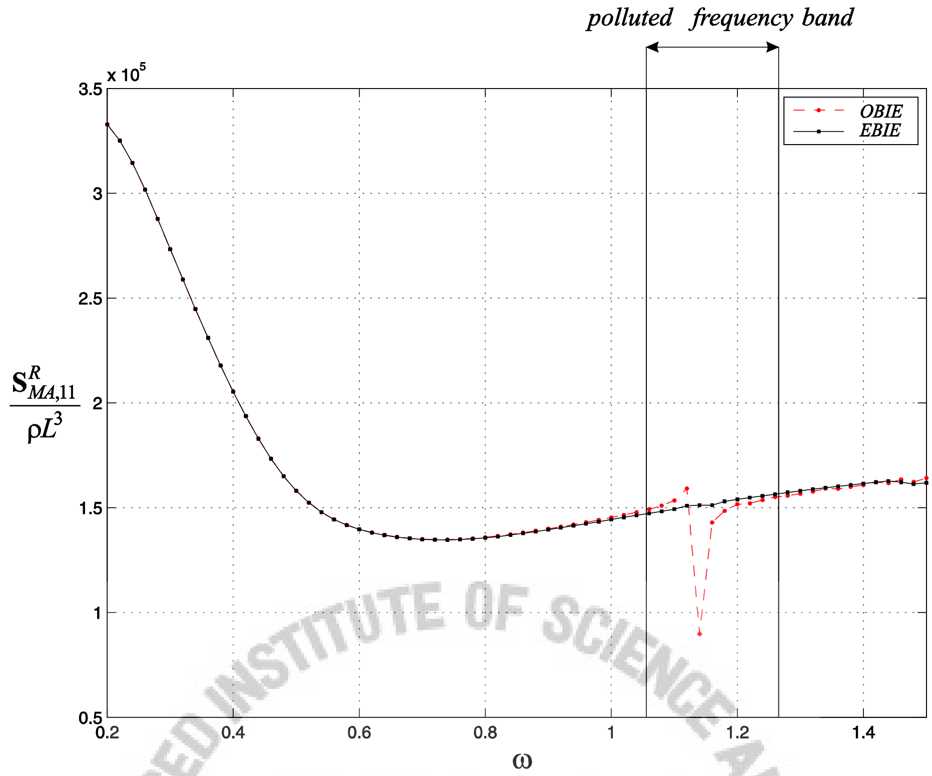

Figure 4.3. Surge added mass of ship-shaped offshore unit as function of wave frequency and the polluted frequency band.

4.1 Comparison of the computational cost between OBIE and EBIE

To carry out the numerical analysis of the interaction of surface wave with floating structure, it is necessary to evaluate the free-surface Green function for each wave frequency. The free-surface Green function contains the integral of which domain goes infinity, so direct numerical evaluation is inefficient. Several algorithms for the free-surface Green function evaluation have been developed [19, 20, 21] to reduce the computational cost, and Newman's algorithm is widely used. The linear system of equations also should be solved for each wave frequency. Both the iterative solver and the direct solver are available. When the degree of freedom is large, it is recommended to use the iterative solver in terms of the computational cost [18] . These two calculations occupy most of the computational cost. It is difficult to calculate the computational cost precisely, because the Green function evaluation and solving the linear system of equation vary with the wet surface of floating structures. Nevertheless, it is evident that the computational cost increases as the degree of freedom increases. Therefore, the EBIE method increases the computational cost, because this method extend its domain. Let's define N^B is the number of node on S_B and N^I is the number of node on S_I. Without the EBIE method, the free-surface Green function must be evaluated for each combination nodes on S_B, that is $\left(N^B\right)^2$ evaluations should be done for single wave frequency. However, with the EBIE method, the number of evaluations increases to $\left(N^B+N^I\right)^2$. The size of linear system of equations that should be solved to obtain a solution increases from N^B to $\left(N^B+N^I\right)$. In Figure 4.4 the relation of degree of freedom on S_B and the number of the Green function evaluation is shown where x-axis means the degree of freedom on S_B, and y-axis means the number of the free-surface Green function evaluation. The number of Green function evaluation is growing according to a quadratic curve. In Figure 4.5 the normalized computational time is plotted in y axis, and the degree of freedom is plotted on S_B. Each computational time is divided by the longest one. Numerical hydrodynamic analysis of barge is carried out for single wave frequency repeatedly using WAMIT as increasing the degree of freedom and higher-order method is used.

Table 4.2. Increment of the number of Green function evaluation and the computational time due to the EBIE method. WAMIT and higer-order method are used.

$N^I/N^B=10\,(\%)$			$N^I/N^B=30\,(\%)$		
N^B	Increment due to EBIE method (%)		N^B	Increment due to EBIE method (%)	
	Number of Green function evaluation	Computational time		Number of Green function evaluation	Computational time
4000		30.52	1920		150.52
5760	21	33.83	4320	69	116.67
7840		33.23	7680		118.17

Table 4.2 gives the increment of the number of Green function evaluation and the computational time corresponding to the degree of freedom on the wet surface. As ratio of N^I to N^B increases, the computational cost increases as expected. Additionally, the increment of the computational cost is larger than the increment of the number of Green function evaluation. This means that not only Green function evaluation but also solving of linear system of equations contribute to the increment of the computational cost.

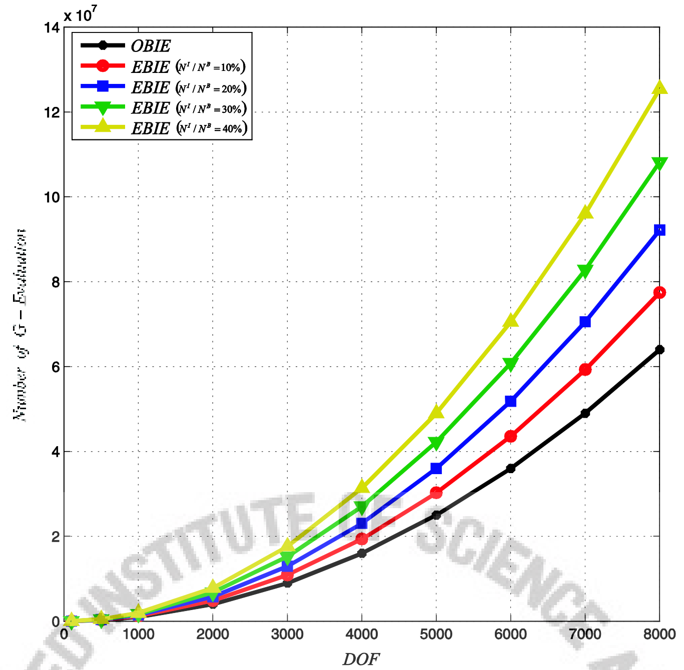

Figure 4.4. Number of the Green function evalution corresponding to the degree of freedom on the wet surface for single wave frequency.

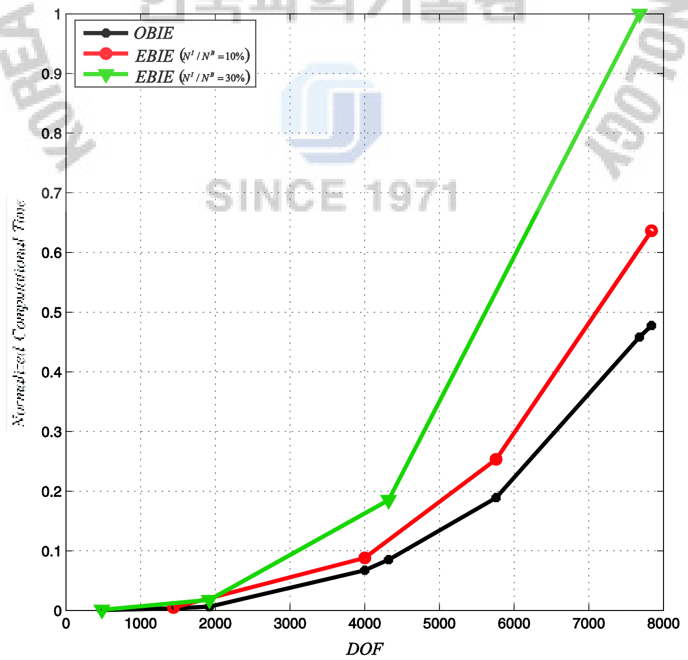

Figure 4.5. Normalized computational time corresponding to the degree of freedom on the wet surface for single wave frequency.

4.2 Criterion for Detecting the Irregular Frequency

As described in section 3.1.5, the irregular frequency affects solution when Equation (3.22) has non-trivial solution. Therefore, if we know whether solution of Equation (3.22) is non-trivial or not for each frequency, we can classify the irregular frequencies that make numerical solution erroneous. This non-trivial solution consist of the sum of the eigenfunctions of eigenvalue problem:

$$2\pi\phi(\mathbf{x}) + \lambda^{eig}\int_{S_B}\left[2\pi\phi(\xi)\left(\frac{1}{2\pi}\frac{\partial G(\mathbf{x};\xi,\omega)}{\partial n(\xi)}\right)\right]dS(\xi) = 0 , \qquad \text{for } \mathbf{x} \text{ on } S_B \tag{4.1}$$

when one of eigenvalues is equal to one that is the parameter of Equation (3.22). In other words, eigenvalue problem (4.1) has the kernel that is a function of frequency, so eigenvalue of problem (4.1) vary with frequency. Then, at certain wave frequencies, one of eigenvalues becomes '1'. In that case, Equation (4.1) becomes equation (3.22), then homogeneous solution of equation (3.22) is sum of eigenfunctions multiplied by arbitrary constants. Therefore, when one of eigenvalues of problem (4.1) becomes '1', equation (3.2) has infinite solution.

This eigenvalue problem can be transformed into generalized matrix eigenvalue problem:

$$\left[2\pi\,\mathbf{F}_M - \lambda^{eig}\,\mathbf{F}_{Gn}(\omega)\right]\hat{\boldsymbol{\varphi}} = \mathbf{0} . \tag{4.2}$$

with variational formulation and boundary element discretization as we derived the discrete linear system of equations. To solve problem (4.1), it is necessary to calculate $\mathbf{F}_M$ and $\mathbf{F}_{Gn}(\omega)$. However, these are calculated in numerical procedure, so additional matrix calculation is not necessary. In addition, we only concern the eigenvalue near '1', so the Arnoldi method that approximate a few eigenvalues and corresponding eigenvectors effectively could be applied.

In the discretized problem, continuous frequency range is also discretized and the linear system of equations are solved for each discrete frequencies. Then, the linear system of equations becomes ill-conditioned near the irregular frequencies. This phenomena can be described in terms of eigenvalue of problem (4.2). As eigenvalue that is a function of frequency approach to '1', a numerical solution becomes erroneous. In order to distinguish the frequency that is affected by the irregular frequency, it is necessary to define a criterion:

$$\left|\lambda^{eig} - 1\right| < \varepsilon , \tag{4.3}$$

and ε depends on the discretization of wet-surface and interpolation order of the boundary element. λ^{eig} is complex, because components of $\mathbf{F}_{Gn}(\omega)$ are complex. Therefore, the criterion (4.3) becomes

$$\left|\mathrm{Re}\left(\lambda^{eig}\right)-1\right|<\varepsilon_{re} \tag{4.4a}$$

$$\left|\mathrm{Im}\left(\lambda^{eig}\right)\right|<\varepsilon_{im}\,. \tag{4.4b}$$

In this thesis, wet-surface is discretized into quadrilateral flat panels of which length is shorter than a quarter of wave length. Under theses conditions, we set ε_{re} and ε_{im} as 0.015 that makes error due to the EIBE method under 5% through numerical tests.

4.3 Cost Reduction Procedure and Its Limitation

Numerical analysis procedure that solve the Exterior Neumann problem with and without the EBIE method are shown in Figure 4.6. Numerical analysis step colored with yellow includes the Green function evaluation and numerical analysis step colored with green includes solving the linear system of equations. As explained, the number of the Green function evaluation and the size of the linear system increases by adapting the EBIE method to remove the irregular frequency effect for every frequency, then the total computational time increases as shown in Fiure. 4.5. Therefore, we suggest the cost reduction procedure for the IRR method that apply the EBIE method selectively by using the criterion presented in the previous section as shown in Figure 4.7.

This procedure, in common with existing numerical analysis procedure, first make mass and hydrostatic stiffness matrices that are already mentioned in Equation (2.29), and then build the fluid matrices: $\mathbf{F}_{Gn}(\omega)$, $\mathbf{F}_{G}(\omega)$, and $\mathbf{R}_{I}(\omega)$ for each wave frequency. While the existing numerical analysis procedure with EBIE method construct added mass and wave damping matrices, and wave force vector (2.29), the cost reduction procedure solve the eigenvalue problem (4.2) and check the criterion (4.4) to identify whether wave frequency is in "polluted" frequency band or not for each wave frequency. When the criterion (4.4) is not satisfied, added mass and wave damping matrices, and wave force vector are calculated according to Equation (2.29). On the other hand, if the criterion (4.4) is satisfied, added mass and wave damping matrices, and wave force vector are calculated by adapting the EBIE method.

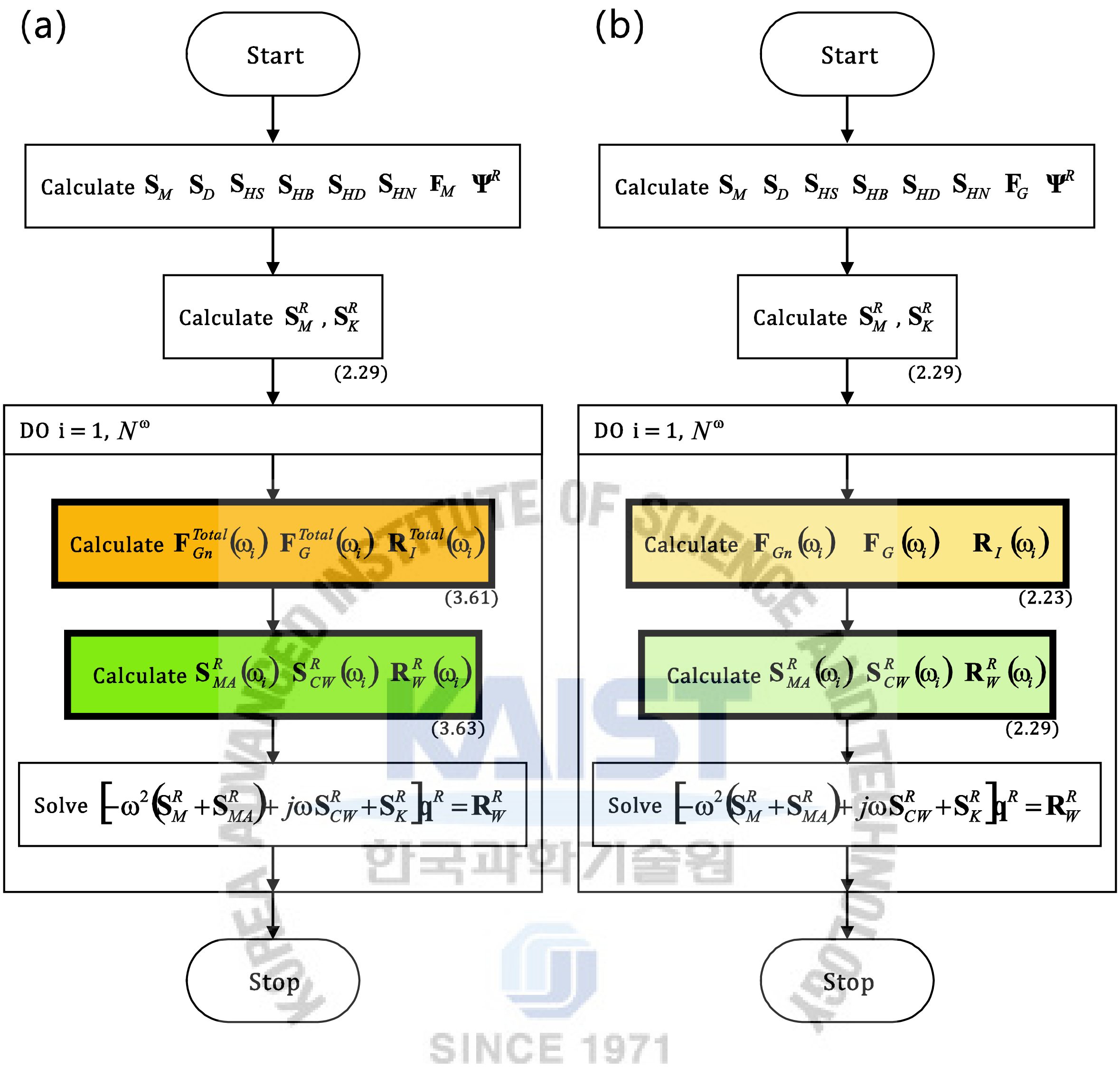

Figure 4.6. Numerical Analysis Procedure (a) with the EBIE method, (b) without the EBIE method. N^ω is the number of wave frequency.

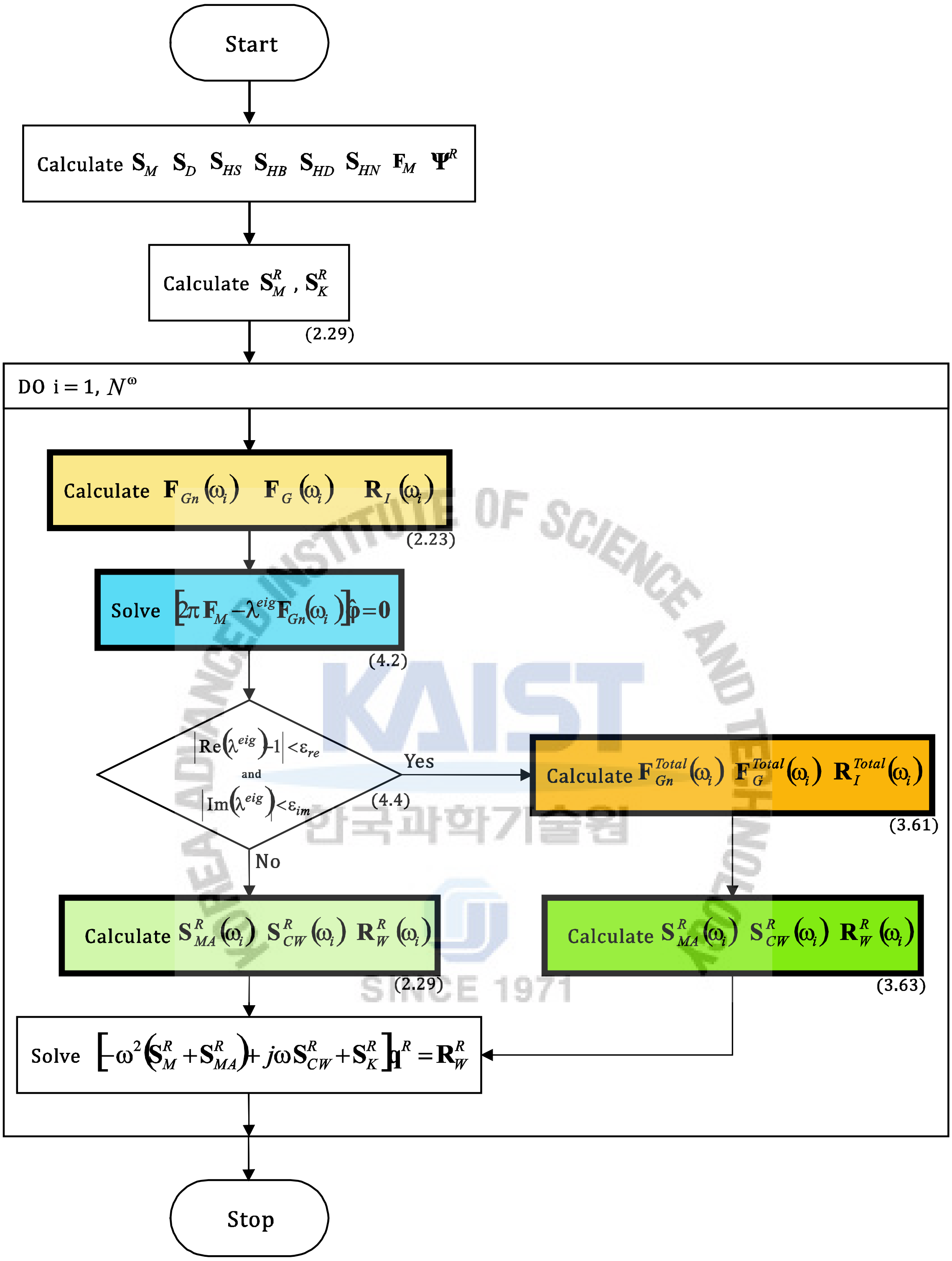

Figure 4.7. Cost reduction procedure for the irregular frequency removal method. N^ω is the number of wave frequency.

The cost reduction procedure need to solve eigenvalue problem for every frequency. Then, if it takes more time than the computational time increase due to the EBIE method, it is meaningless procedure. We use the Arnoldi method [22] to compute one eigenvalue closest to '1', and computational time of it also increases as degree of freedom increases. The computational time of eigenvalue problem is relatively small compared to the increment of the computational time due to the EBIE method for single frequency analysis as shown in Figure. 4.8. Figure 4.8 is equal to Figure 4.5, but include the computational time of eigenvalue analysis using Arnoldi method additionally.

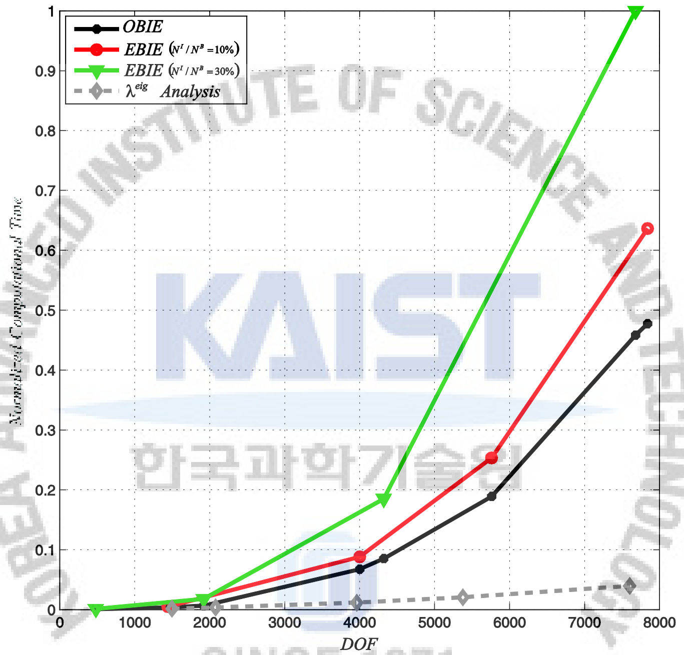

Figure 4.8. Computational cost of OBIE method, EBIE method, and Eigenvalue problem corresponding to the degree of freedom on the wet surface.

Another point should be considered is the number of frequencies that is classified according to the criterion (4.4). Present procedure could be effective when a few of frequencies are affected in the frequency range of interest. Fortunately, it is well known that general shape of ships has a few irregular frequencies and if wet-surface discretization is enough, "polluted" frequency bandwidth is relatively small. Therefore, present procedure could be effective for hydrodynamic analysis of ships and ship shaped floating structures.

In this section, we present the cost reduction procedure for IRR method that adapt the EBIE method selectively. This procedure could be effective when the number of wave frequency that are affected by the irregular frequency are relatively small, and the computational cost of solving the eigenvalue problem (4.2). To verity the effectiveness of the cost reduction procedure, examples of barge, circular cylinder, and ship-shaped offshore unit are presented in the next chapter.

Chapter 5. Numerical Results

In this chapter, we consider three examples: barge, circular cylinder, and ship-shaped offshore unit. We validate the criterion (4.4) that separate out frequencies that are in polluted solution bandwidth by comparing with analytical irregular frequencies of barge and circular cylinder in the frequency range of interest. The added mass, and excitation force are calculated and eigenvalue problem (4.2) is solved in frequency range from 0.2 to 3.0 rad/s. We show the feasibility of the cost reduction procedure by applying to the ship-shaped offshore unit.

5.1 Barge

The barge of which the length L is 10m, the breadth B is 10m, and the draft T is 2m is considered. The irregular frequencies that are in frequency range from 0.2 to 3.0 rad/s are 2.48 and 2.79 rad/s. The discretization of barge is shown in Figure 4.1. Figure 4.2 and 4.3 show the added mass, the wave excitation forces on the barge for the surge and heave modes, and one of eigenvalues that is closest to '1' of the eigenvalue problem (4.2) respectively. As eigenvalue approach to '1', a solution becomes erroneous, and its point corresponds with the irregular frequencies well. Therefore, it is shown that the criterion (4.4) presented in the previous chapter is applicable to separate out the frequencies that are affected by the irregular frequencies.

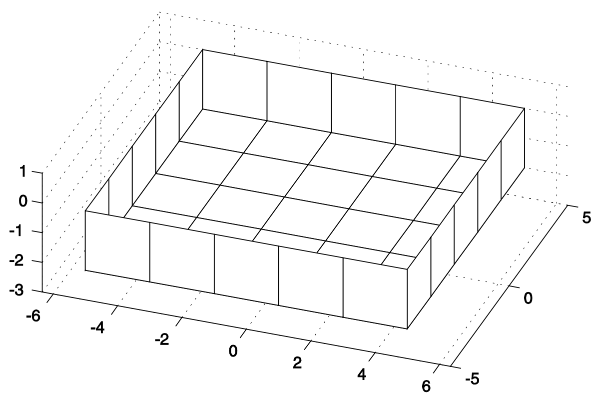

Figure 5.1. Discretization of Barge.

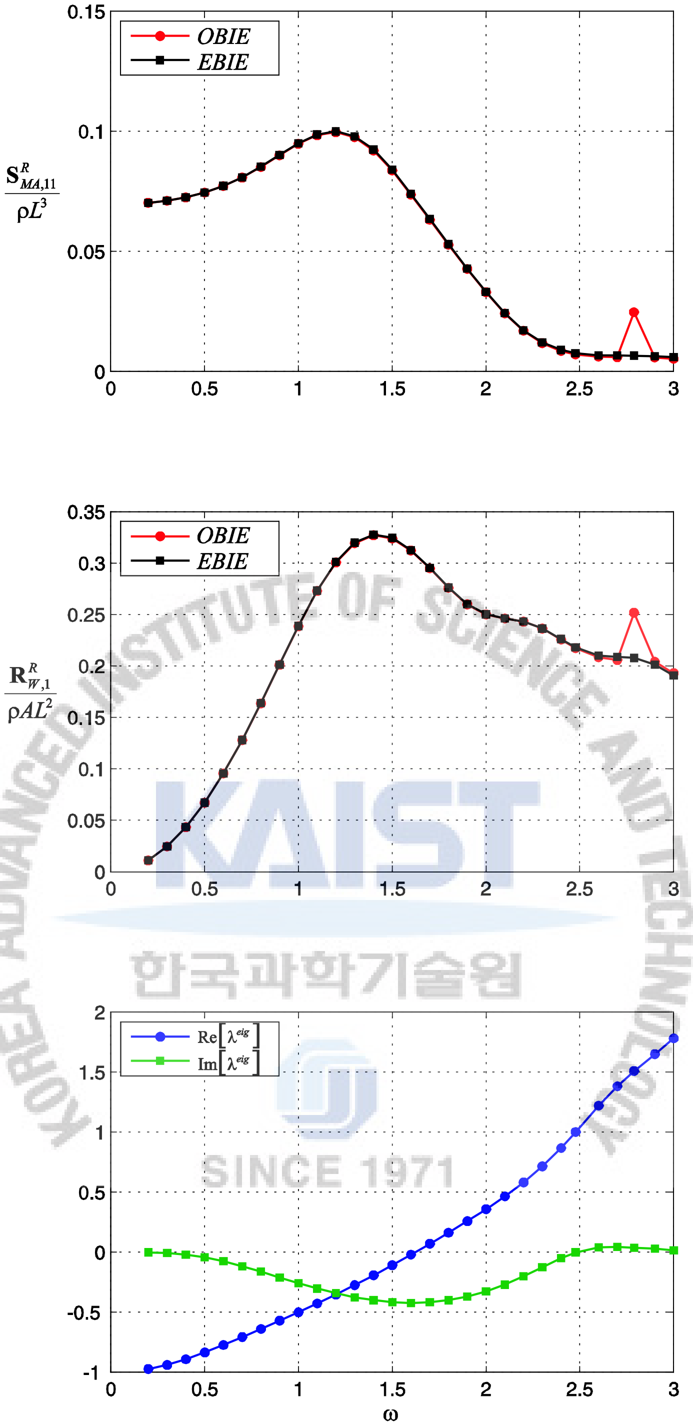

Figure 5.2. Surge added mass, wave excitation force on the barge and eigenvalue of problem (4.2) as function of wave frequency. L is the length of barge, and A is the amplitude of the incident wave. Added mass and wave excitation force are non-dimensionalized by ρL^3 and $\rho A L^2$ where ρ is the water density.

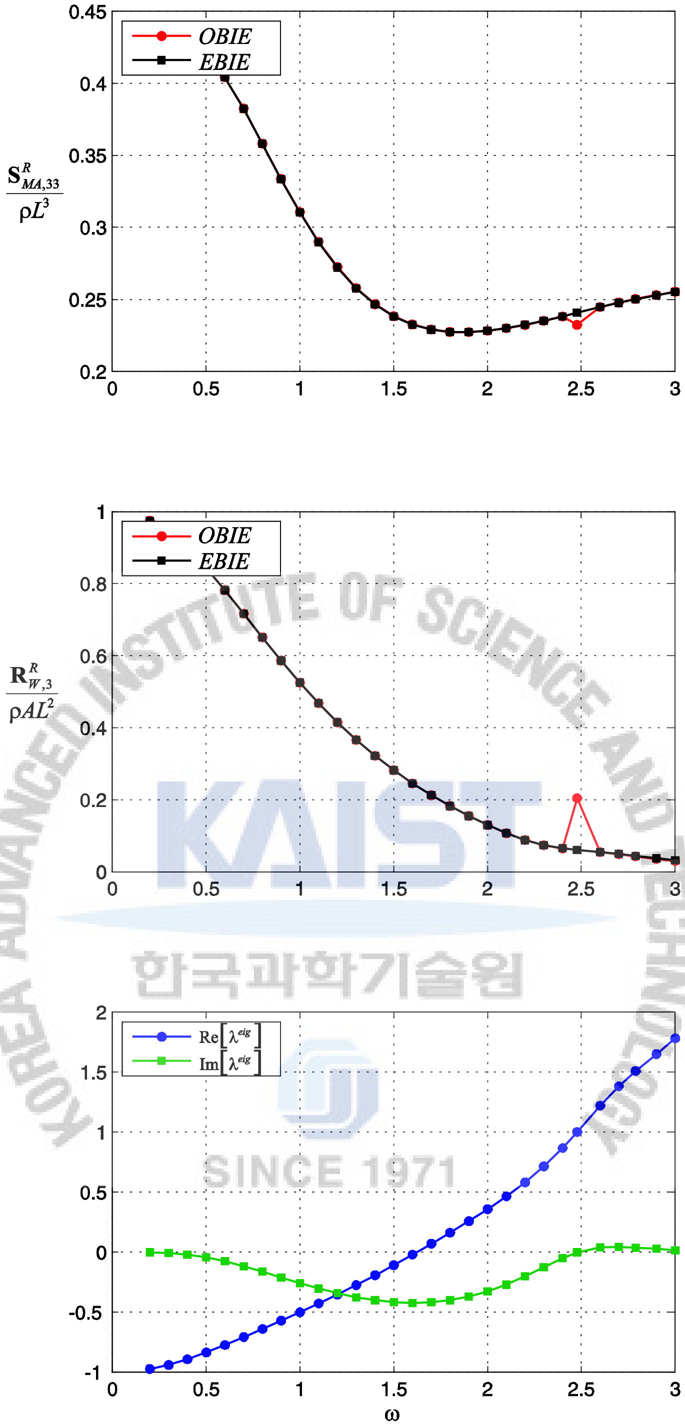

Figure 5.3. Heave added mass, wave excitation force on the barge and eigenvalue of problem (4.2) as function of wave frequency. Other definitions are equal to those of Figure 5.2.

5.2 Circular Cylinder

The circular cylinder of which the radius L is 4m, and the draft T is 2m is considered. The irregular frequency that are in frequency range from 0.2 to 3.0 rad/s is 2.66 rad/s. The discretization of circular cylinder is shown in Figure 5.4. Figures 5.5 and 5.6 show the added mass, the wave excitation forces on the circular cylinder for the surge and heave modes, and one of eigenvalues that is closest to '1' of the eigenvalue problem (4.2) respectively. In common with barge case, circular cylinder results show that the criterion presented in the previous chapter is applicable.

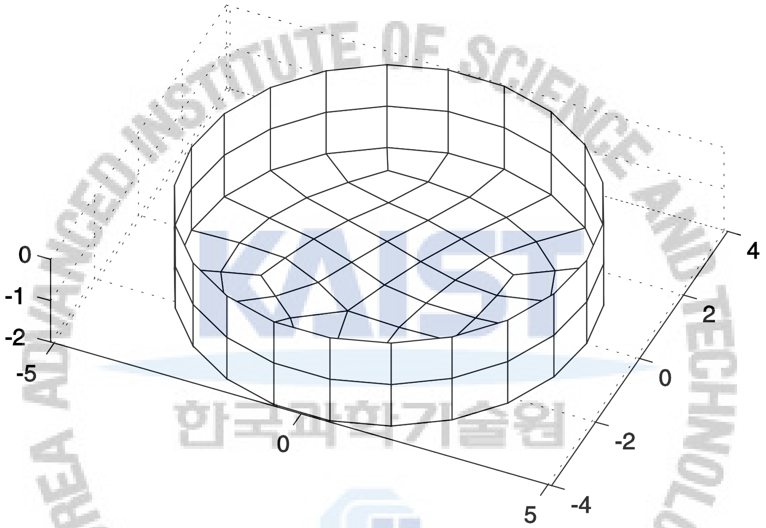

Figure 5.4. Discretization of circular cylinder.

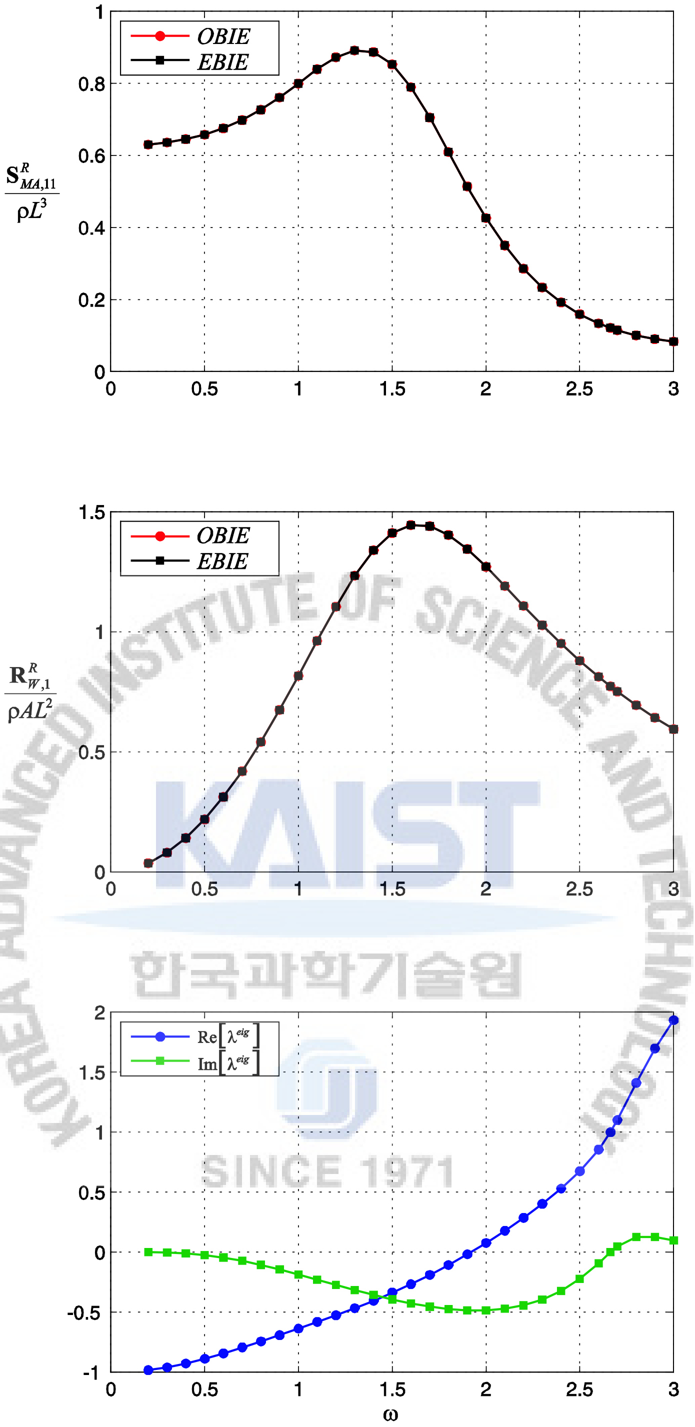

Figure 5.5. Surge added mass, wave excitation force on the circular cylinder and eigenvalue of problem (4.2) as function of wave frequency. L is the radius of circular cylinder, and A is the amplitude of the incident wave. Added mass and wave excitation force are non-dimensionalized by ρL^3 and $\rho A L^2$ where ρ is the water density.

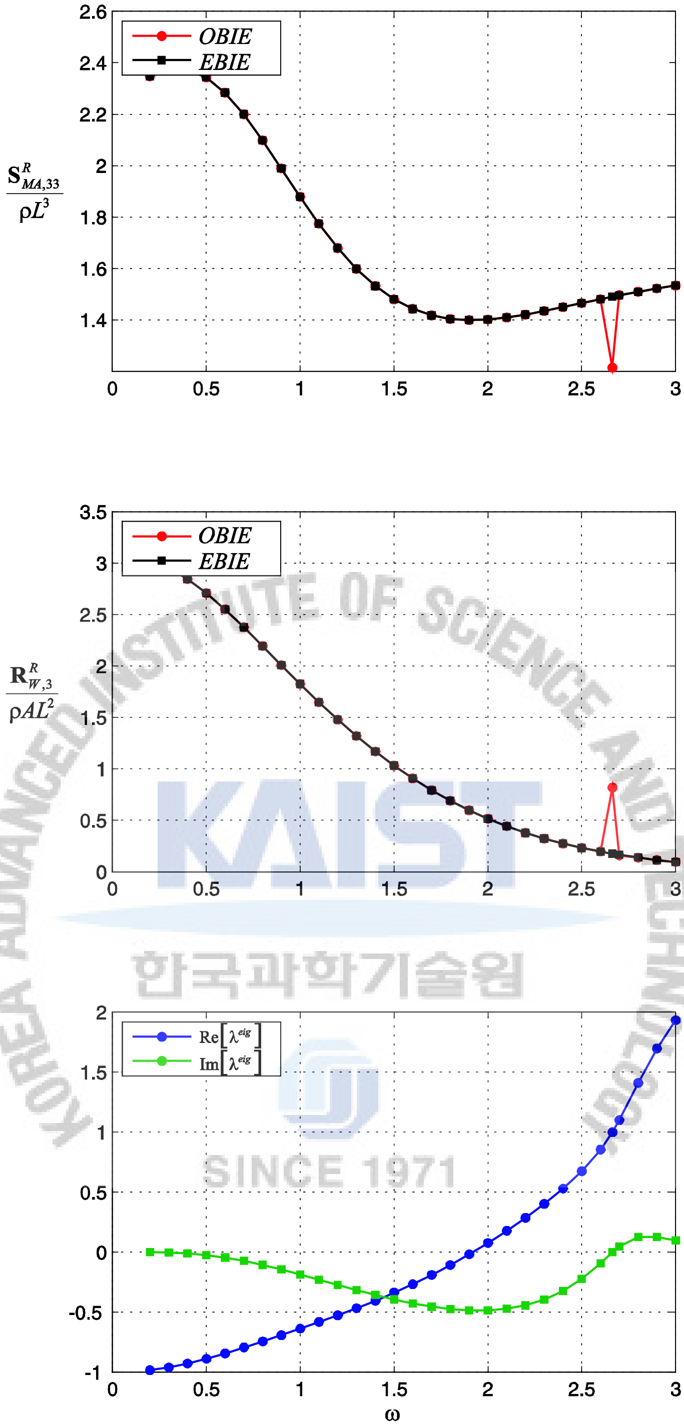

Figure 5.6. Heave added mass, wave excitation force on the circular cylinder and eigenvalue of problem (4.2) as function of wave frequency. Other definitions are equal to those of Figure 5.5.

5.3 Ship-shaped offshore unit

Ship-shaped offshore unit shown in Figure 5.7 is considered in order to show feasibility of the cost reduction procedure for IRR method. Numerical analysis conditions and results are shown in Table 5.1. Panel model of ship-shaped offshore unit is equal to model that is presented in chapter 4, but the interior free-surface panel is generated manually not by applying option of WAMIT. Through the cost reduction procedure, 8 frequencies out of 81 frequencies are considered as being affected by the irregular frequencies and 29.3% computational cost is saved in comparison with numerical analysis procedure with EBIE method. Figures 5.8, 5.9, and 5.10 show the added mass, the wave radiation damping on ship-shaped offshore unit for the surge, heave, and roll modes, and one of eigenvalues that is closest to '1' of the eigenvalue problem (4.2) respectively.

Table 5.1. Analysis conditions and computational times of ship-shaped offshore unit using the numerical analysis procedure with EBIE method and the cost reduction procedure that is presented in the chapter 5. Wave angle is defined in Figure 2.1.

Degree of Freedom		Wave Condition		Computational time (s)	
N^B	N^I	Angle (rad)	Frequency (rad/s)	Numerical analysis procedure with EBIE method	Cost reduction procedure
1401	369	0	0.2 ~ 1.8	5629.5	3978.2

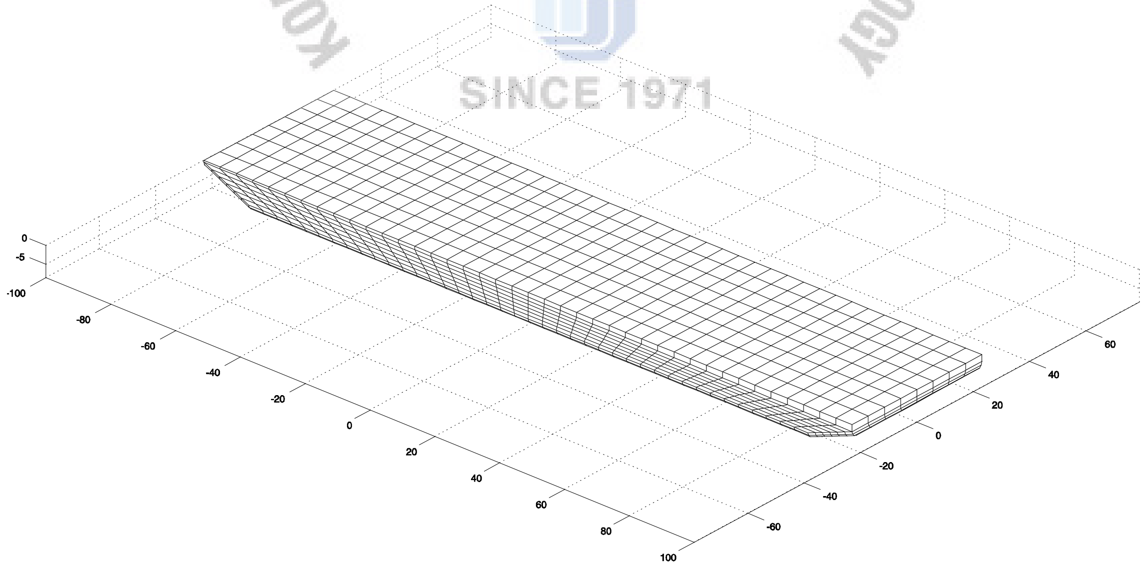

Figure 5.7. Discretization of Discretization of ship-shaped offshore unit.

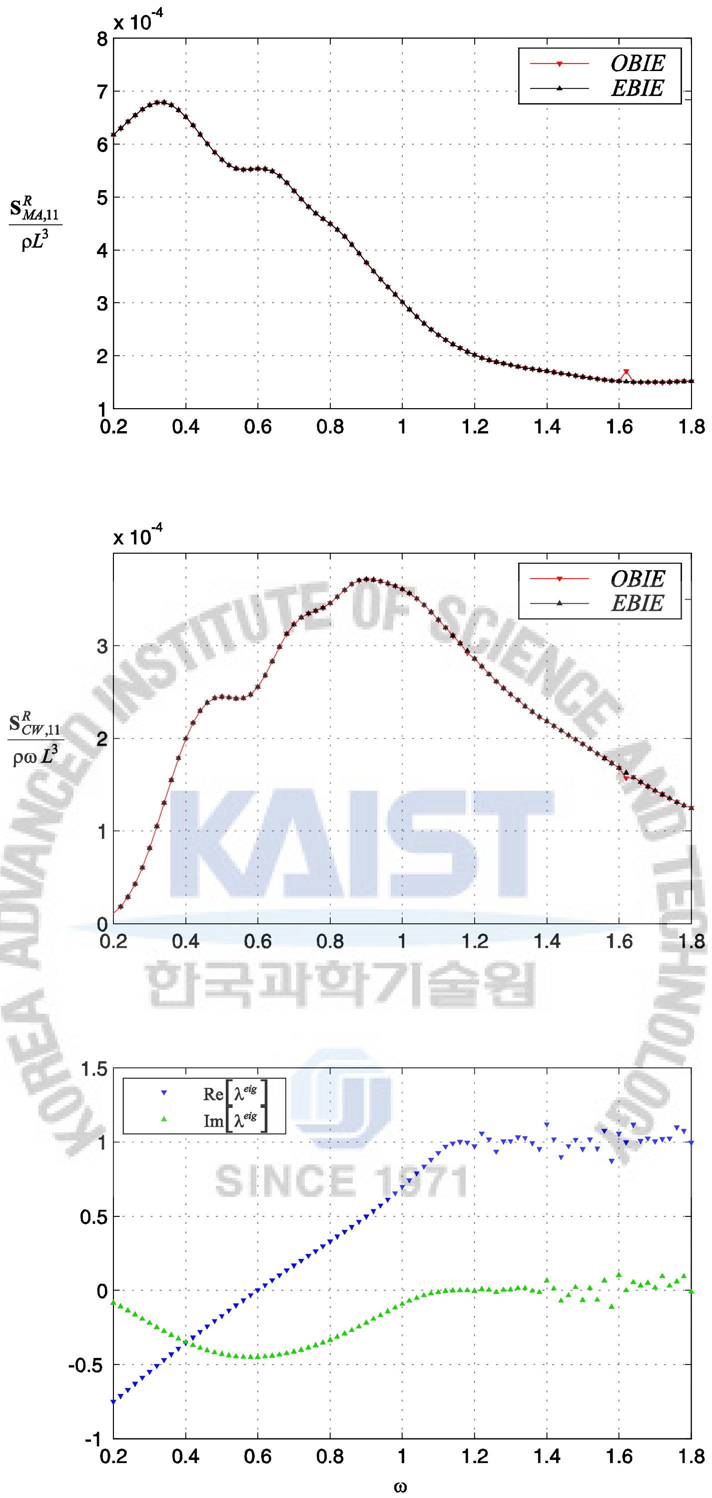

Figure 5.8. Surge added mass, wave damping on ship-shaped offshore unit and eigenvalue of problem (4.2) as function of wave frequency. L is the length of ship-shaped offshore uint. Added mass and wave damping are non-dimensionalized by ρL^3 and $\rho\omega L^3$ where ρ is the water density.

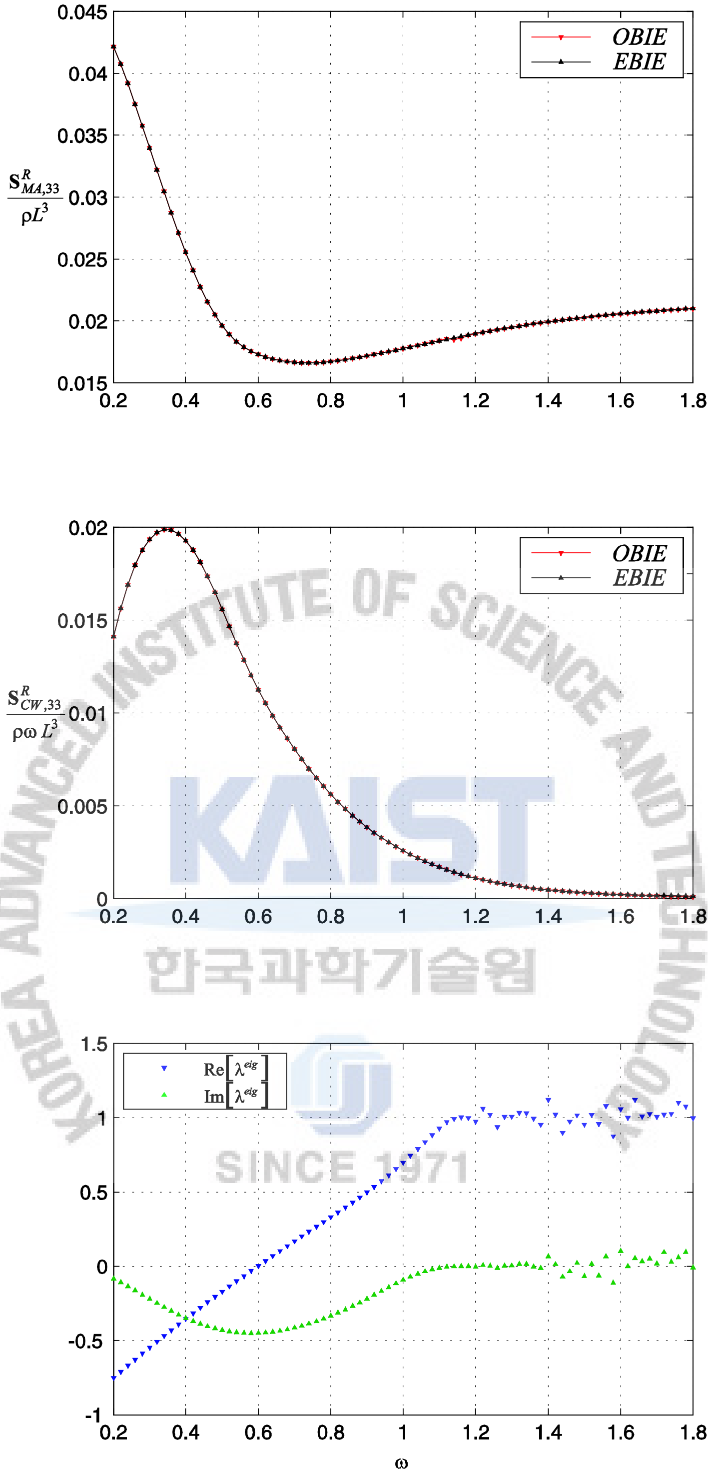

Figure 5.9. Surge added mass, wave damping on ship-shaped offshore unit and eigenvalue of problem (4.2) as function of wave frequency. Other definitions are equal to those of Figure 5.8.

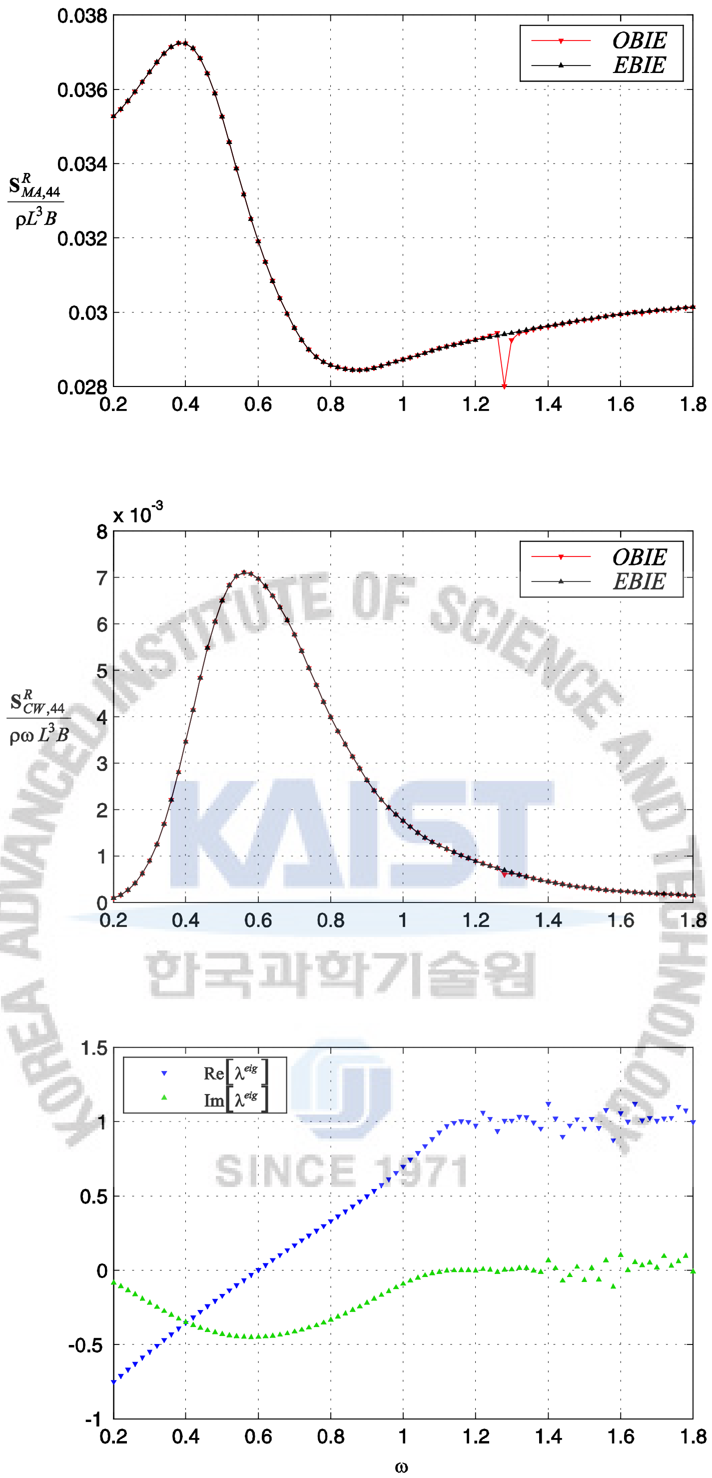

Figure 5.10. Roll added mass, wave damping on ship-shaped offshore unit and eigenvalue of problem (4.2) as function of wave frequency. L and B are the length and breadth of ship-shaped offshore uint, repectively. Added mass and wave damping are non-dimensionalized by $\rho L^3 B$ and $\rho\omega L^3 B$ where ρ is the water density.

Chapter 6. Conclusions

We define the irregular frequencies of the boundary integral equation that representing the exterior Neumann problem. With the Fredholm's theorems, we investigate the cause of the irregular frequencies, and review the irregular frequency removal method have been developed briefly. Each method has its pros and cons, and the extended boundary integral equation method is the only way to remove the irregular frequency effect for three dimensional floating structure of arbitrary shape. However, the computational cost increase depending on the discretization of the interior free-surface. Therefore, it is necessary to reduce the computational cost, and we present the cost reduction procedure for IRR method that adapt the extended boundary integral equation method selectively. To distinguish the frequencies that are affected by the irregular frequencies, the cost reduction procedure needs to solve the eigenvalue problem. We adopt the Arnoldi method for eigenvalue problem, and it is shown that the computational time of eigenvalue problem is relatively small compared to the increment of the computational time due to the EBIE method for single frequency. In case of the barge and the circular cylinder of which the irregular frequencies can be derived analytically, frequencies are in "polluted" freqeuncy band are detected appropriately by adapting the cost reduction procedure. We also apply the cost reduction procedure for ship-shaped offshoure unit, and it save 29.3% computational cost in comparison with the numerical analysis procedure with EBIE method.

In this research, we present the cost reduction procedure for IRR method to reduce the computational cost. It is expected that this procedure is effective especially to deal with large degree of freedom problem. However, it is applicable when single floating structure is considered and it would be effective only when the number of frequencies affected by the irregular frequencies in the frequency range of interest is relative small.

References

[1] Zhu, X. (1994). "Irregular Frequency Removal from the Boundary Integral Equation for the Wave-Body Problem", *M.S. Thesis*, Massachusetts Institute of Technology.

[2] Lamb, H. (1916). *Hydrodynamic*, Cambridge University Press.

[3] John, F. (1949). "On the Motion of Floating Bodies Ⅰ,Ⅱ." *Communication on Pure and Applied Mathematics*, 2(1).

[4] Lau, S. M. and Hearn, G. E. (1989), "Suppression of irregular frequency effects in fluid–structure interaction problems using a combined boundary integral equation method." *Int. J. Numer. Meth. Fluids*, 9(2), pp. 763-782.

[5] Ursell, F. (1981), "Irregular frequencies and the motion of floating bodies." *Journal of Fluid Mechanics*, 105, pp. 143-156.

[6] Zhu, X., Lee, C.H. (1994), "Removing the Irregular Frequencies in Wave-Body Interactions." *9th International Workshop on Water Waves and Floating Bodies (IWWWFB09)*, Kuju, Fukuoka, Japan, pp. 245-249.

[7] Kim, K.-T., Lee, P.-S. and Park, K. C. (2013), "A direct coupling method for 3D hydroelastic analysis of floating structures." I*nt. J. Numer. Meth. Engng*, 96(13), pp. 842-866.

[8] Yoon, J. S., Cho, S. P., Jiwinangun, R. G., & Lee, P. S. (2014). "Hydroelastic analysis of floating plates with multiple hinge connections in regular waves." *Marine Structures*, 36, pp. 65-87.

[9] Dalrymple, R. A., & Dean, R. G. (1991). *Water wave mechanics for engineers and scientists*. Prentice-Hall.

[10] Wehausen, J.V., and Laitone, E.V. (1960), "Surface waves." *Encyclopedia of Physics*, 9, pp. 446-778.

[11] Newman, J.N. (1977). *Marine Hydrodynamics*, The MIT press.

[12] Bathe, K.J. (1996). *Finite Element Procedures*, Prentice Hall.

[13] Ram P, K. (1971). *Linear Integral Equations-Theory and Technique*, Academic Press.

[14] Hong, D. C. (1987). “On the improved Green integral equation applied to the water-wave radiation-diffraction problem.” *J Soc Nav Archit Korea*, 24, pp 1-8.

[15] Sayer, P., and Ursell, F. (1977) "Integral-equation methods for calculating the virtual mass in water of finite depth." *Proc. 2nd Int. Symp. Numerical Hydro*. University of California.

[16] Martin, P. A. (1981). “On the null-field equations for water-wave radiation problems.” *Journal of Fluid Mechanics*, 113, pp. 315-332.

[17] Lee, C. H., Newman, J. N., & Zhu, X. (1996). “An extended boundary integral equation method for the removal of irregular frequency effects.” *International Journal for Numerical Methods in Fluids*, 23(7), pp. 637-660.

[18] Lee, C. H., & Newman, J. N. (2006). *WAMIT® User Manual, Versions 6.3, 6.3 PC, 6.3 S, 6.3 S-PC. Chestnut Hill*, MA: WAMIT.

[19] Newman, J. N. (1985). “Algorithms for the free-surface Green function.” *Journal of Engineering Mathematics*, 19(1), pp. 57-67.

[20] Telste, J. G., & Noblesse, F. (1986). “Numerical evaluation of the Green function of water-wave radiation and diffraction.” *Journal of ship research*, 30(2), pp. 69-84.

[21] Yang, S. A. (2000). “On the singularities of Green's formula and its normal derivative, with an application to surface-wave–body interaction problems.” *International Journal for Numerical Methods in Engineering*, 47(11), pp. 1841-1864.

[22] Sorensen, D. C. (1992). “Implicit application of polynomial filters in ak-step Arnoldi method.” *SIAM Journal on Matrix Analysis and Applications*, 13(1), pp. 357-385.

요 약 문

파랑-구조 상호작용 문제에서

비정상 주파수 현상 검출

파랑-구조 상호작용 문제는 조선 및 해양공학에서 자주 다루어지는 문제이며, 포텐셜 이론이 해석을 위해 사용되어왔다. 특히 선형화된 자유표면 경계조건을 만족하는 그린 함수를 이용한 주파수영역 수치 해석 방법은 부유체 운동 해석에 널리 사용되며, 이와 관련된 많은 연구들이 수행되어오고 있다. 하지만 해석하는 부유체의 크기가 커지고, 형상이 다양에 짐에 따라 특정 주파수에서 큰 오차가 발생한다. 이 현상이 일어나는 주파수를 비정상 주파수라 하며, 이를 제거하기 위한 많은 방법이 개발되어왔다.

비정상 주파수 현상은 물리적 현상이 아니라 수학 모델링 과정에서 발생하는 현상이다. 이를 제거하기 위한 방법은 초기 이차원 문제에만 적용이 가능한 방법부터 삼차원의 일반적인 형상까지 적용이 가능반 EBIE 방법까지 개발이 되어왔다. EBIE 방법을 부유체 운동해석에 많이 적용해오고 있으나, 수치해석에 필요한 시간이 증가하는 문제가 있다.

본 연구에서는 EBIE 을 선택적으로 적용하여 수치해석 시간을 줄이는 절차를 제시하였다. 주파수 영역 해석에서 비정상 주파수의 영향을 받는 주파수를 판별하는 기준을 제시하고, 이 기준을 이용한 해석 절차를 제시하였다. 비정상 주파수를 이론적으로 계산할 수 있는 직육면제와 원형 실린더에 적용하여 비정상 주파수 검출의 가능성을 입증하였다. 또한 선박형태의 해양구조물에도 제시한 수치해석 절차를 적용하여 수치 해석 시간의 절약 가능성을 보였다.

핵심어: 파랑-구조 상호작용; 포텐셜 이론; 경계 적분 방정식; 자유표면 그린함수; 비정상 주파수